A TRIDENT SCHOLAR PROJECT REPORT

NO. 237

"WAVE INTERACTIONS WITH VERTICAL WAVE BARRIERS"

UNITED STATES NAVAL ACADEMY
ANNAPOLIS, MARYLAND

This document has been approved for public release and sale; its distribution is unlimited.

DTIC QUALITY INSPECTED 1

20000406 107

REPORT DOCUMENTATION PAGE

Form Approved
OMB No. 0704-0188

Public reporting burden for this collection of information is estimated to average 1 hour per response, including the time for reviewing instructions, searching existing data sources, gathering and maintaining the data needed, and completing and reviewing the collection of information. Send comments regarding this burden estimate or any other aspect of this collection of information, including suggestions for reducing this burden, to Washington Headquarters Services, Directorate for Information Operations and Reports, 1215 Jefferson Davis Highway, Suite 1204, Arlington, VA 22202-4302, and to the Office of Management and Budget Paperwork Reduction Project (0704-0188), Washington DC 20503.

1. AGENCY USE ONLY (*Leave Blank*)	2. REPORT DATE	3. REPORT TYPE AND DATES COVERED
	1996	

4. TITLE AND SUBTITLE

Wave interactions with vertical wave barriers

5. FUNDING NUMBERS

6. AUTHOR(S)

Bollmann, Chad A.

7. PERFORMING ORGANIZATION NAME(S) AND ADDRESS(ES)

8. PERFORMING ORGANIZATION REPORT NUMBER

9. SPONSORING/MONITORING AGENCY NAME(S) AND ADDRESS(ES)

United States Naval Academy
Annapolis, MD 21402

10. SPONSORING/MONITORING AGENCY REPORT NUMBER

USNA Trident Scholar report; no. 237 (1996)

11. SUPPLEMENTARY NOTES

Accepted by the U.S.N.A. Trident Scholar Committee

12a. DISTRIBUTION/AVAILABILITY STATEMENT

Approved for public release; distribution unlimited.

12b. DISTRIBUTION CODE

UL

13. ABSTRACT (*Maximum 200 words*)

Vertical wave barriers, also known as vertical wall breakwaters, are designed to reduce the amount of wave energy behind the barrier to allow the safe mooring of vessels. These structures are constructed of wooden or concrete panels mounted to piles. The panels extend from above the water surface down to approximately mid-depth, leaving a gap near the sea floor. The existing procedures used to design vertical wave barriers remain essentially unchanged since 1960. These procedures produce uncertainties when used to predict transmitted wave height and wave loading (force) on the barriers; it is hoped that new approaches developed in this project may be adopted into modern design guidelines. The theoretical approach of this investigation involved modification of existing linear wave theory to account for the effects of reflected waves. This resulted in a new theory for both wave transmission and for wave forces on the barrier. Wave transmission and reflection and resultant forces were measured when a model wave barrier was subjected to regular and irregular (random) waves. Additionally, flow characteristics underneath the breakwater were measured. With the recorded data the new theories can be verified and substantial forward progress can be made in the design procedures for these barriers.

14. SUBJECT TERMS

Wave barrier Wave screen Vertical wall breakwater

15. NUMBER OF PAGES

84

16. PRICE CODE

17. SECURITY CLASSIFICATION OF REPORT	18. SECURITY CLASSIFICATION OF THIS PAGE	19. SECURITY CLASSIFICATION OF ABSTRACT	20. LIMITATION OF ABSTRACT
UNCLASSIFIED	UNCLASSIFIED	UNCLASSIFIED	UL

U.S.N.A. --- Trident Scholar project report; no. 237 (1996)

"WAVE INTERACTIONS WITH VERTICAL WAVE BARRIERS"

by

Midshipman Chad A. Bollmann, Class of 1996
United States Naval Academy
Annapolis, Maryland

(signature)

Certification of Adviser Approval

Associate Professor David L. Kriebel
Naval Architecture, Ocean, and Marine Engineering Department

(signature)

3 May 96
(date)

Acceptance for the Trident Scholar Committee

Professor Joyce E. Shade
Chair, Trident Scholar Committee

(signature)

6 May 1996
(date)

USNA-1531-2

ABSTRACT

Vertical wave barriers, also known as vertical wall breakwaters, are designed to reduce the amount of wave energy behind the barrier to allow the safe mooring of vessels. These structures are constructed of wooden or concrete panels mounted to piles. The panels extend from above the water surface down to approximately mid-depth, leaving a gap near the sea floor. The existing procedures used to design vertical wave barriers remain essentially unchanged since 1960. These procedures produce uncertainties when used to predict transmitted wave height and wave loading (force) on the barriers; it is hoped that new approaches developed in this project may be adopted into modern design guidelines.

The theoretical approach of this investigation involved modification of existing linear wave theory to account for the effects of reflected waves. This resulted in a new theory for both wave transmission and for wave forces on the barrier. Wave transmission and reflection and resultant forces were measured when a model wave barrier was subjected to regular and irregular (random) waves. Additionally, flow characteristics underneath the breakwater were measured. With the recorded data the new theories can be verified and substantial forward progress can be made in the design procedures for these barriers.

Keywords: Wave Barrier, Wave Screen, Vertical Wall Breakwater

TABLE OF CONTENTS

		Page
I.	Abstract	1
II.	Table of Contents	2
III.	Introduction	3
IV.	Background	10
V.	Literature Review	
	Wave Transmission	18
	Forces on Vertical Wave Barriers	23
	Research Objectives	28
VI.	Theory	
	Power Transmission	30
	Modified Transmission Theory	34
	Modified Force Theory	38
VII.	Experimental Setup	
	General Setup	42
	Scaling Laws	44
	Model Construction	46
	Experimental Conditions	50
VIII.	Experimental Results	
	Wave Transmission -- Regular Waves	56
	Wave Transmission -- Random Waves	61
	Wave Forces -- Regular Waves	66
	Underwall Flow Testing	71
	Vortex Flow Testing	75
IX.	Conclusion	78
X.	Acknowledgments	80
XI.	References	81

INTRODUCTION

Recently, there has emerged a renewed interest among ocean engineers in vertical, thin "wave barriers" as a lower-cost breakwater option to protect small recreation and fishing harbors. These breakwaters are generally constructed of sheets or panels of rigid material attached to vertical piles which are embedded in the ocean floor, as shown in Figure 1. The sheets of material extend only partially to the sea floor, leaving a gap between the bottom of the breakwater and the sea floor. Unlike conventional rubble mound breakwaters, which are built with a trapezoidal cross-section, wave barriers or wave "screens" are economically feasible in intermediate depths of water ranging from 30 to 60 feet. This type of breakwater is well-suited for wave protection in areas subject to waves of about three feet (one meter) in height with periods of less than six seconds. A vertical wall breakwater can typically be built for about 1/3 of the $10,000 per foot that rubble mound breakwaters can cost. (Gilman and Nottingham, 1992). A primary advantage of vertical wave barriers is that water can circulate underneath the breakwater, helping to maintain harbor cleanliness and water quality. This design does not completely prevent wave transmission, however, so care must be taken to extend the wall to sufficient depth to limit wave heights within the harbor to an acceptable level.

The specific design and material composition of wave barriers depends on the decisions of the designing engineer when taking the local environment, application, and cost into consideration. In the Seattle Waterfront Project (Gilman, 1995) for instance, the wave barrier is constructed of concrete panels that are attached to vertical steel piles. These

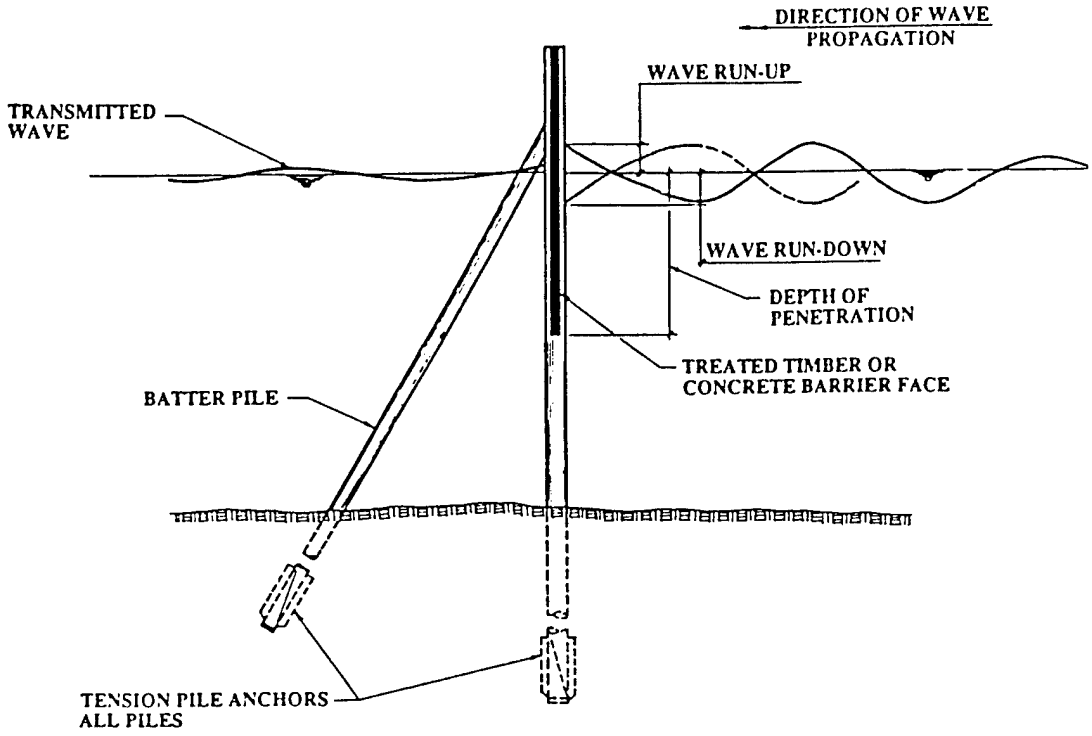

Figure 1. Diagram of vertical wave barrier from Peratrovich, Nottingham, and Drage, Inc., (Issue #39, undated).

vertical piles are, in turn, connected to a pier composed of vertical and batter piles and a concrete cap as shown in Figure 2. This design occupies minimal area within the harbor, supports a pier deck, and allows ships to be tied-up alongside the breakwater [Peratrovich, Nottingham, and Drage, Inc. (PN&D), Issue #39, undated). The Coast Guard's Tillamook Station in Garibaldi, Oregon, is protected by a combination steel and wood breakwater. This breakwater is designed to withstand waves with periods up to five seconds and is actually slanted at an angle to the sea floor. (Gilman and Nottingham, 1992). A wave barrier similar to the Tillamook barrier is shown in Figure 3.

Vertical wave barriers were conceived based on the theory that most of the energy of a wave is concentrated near the water surface. The kinetic energy within a wave rapidly decays as depth increases. The fluid particle velocities, and hence wave energy, decrease to nearly zero at a point one-half of the wave length below the surface of the water, a depth sometimes referred to as the "wave base" (Figure 4). If a wave has a wave base deeper than the depth that the breakwater extends beneath the water surface (penetration), then some amount of wave energy will pass under the breakwater. The amount of transmission depends on the disparity between these two values of breakwater penetration and one-half of the wave length; the greater the difference, the greater the transmission.

There was considerable research done on wave barriers in the 1950s and '60s. However, they have not been widely used or studied in the past 30 years. Nearly all existing theory concerning the interaction of waves with partial vertical wall breakwaters is derived from a paper by Wiegel (1960) which outlines a simplified theory for the transmission of waves by these breakwaters. The theory to predict wave forces on wave barriers was

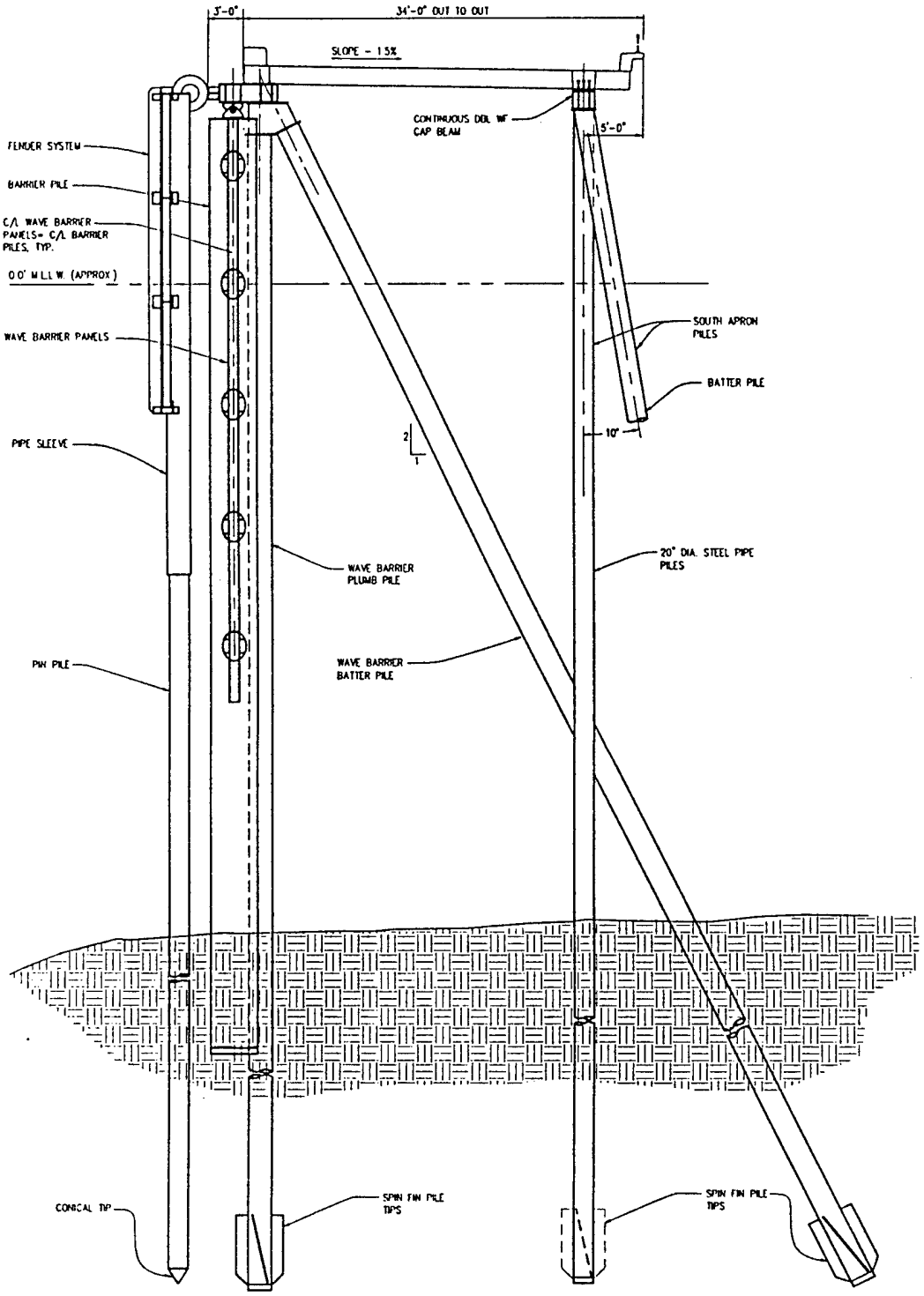

Figure 2. Side view of Seattle Central Waterfront Project wave barrier, PN&D (Gilman, 1995).

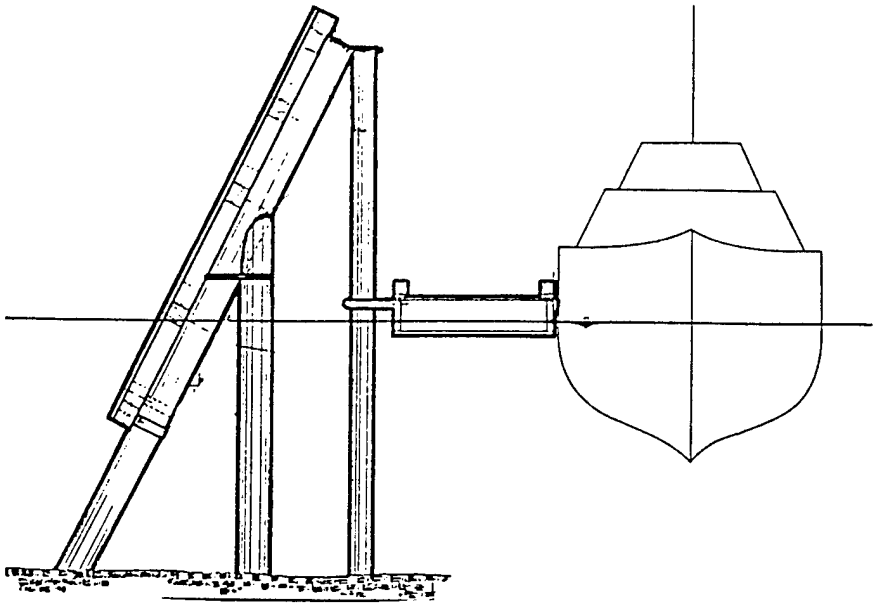

Figure 3. Side view of wave barrier similar to that at Tillamook Coast Guard Station, PN&D (Issue #30, undated).

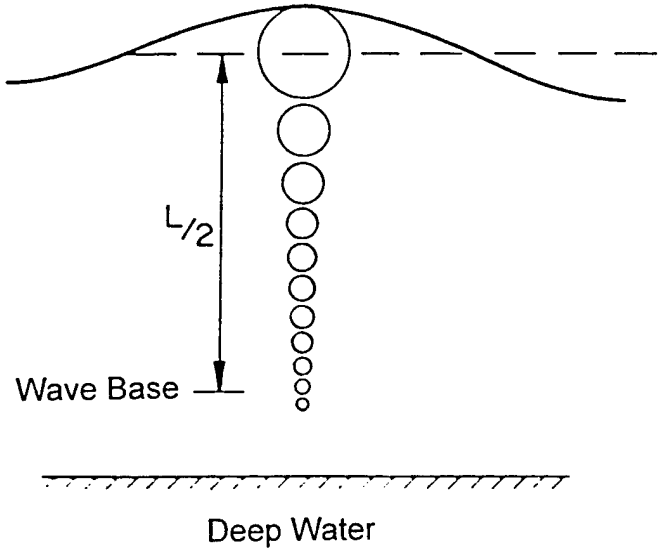

Figure 4. Diagram of deep water wave base. Water particle orbits and wave energy decrease with depth. Sorenson (1993), pp. 16.

developed by Sainflou (1928) and Miche (1944). Rundgren (1958) made experimental observations and later modified Miche's higher-order wave theory. The Sainflou (1928) and Miche-Rundgren (1958) theories are currently used by the Army Corps of Engineers (1984) in their *Shore Protection Manual*. This manual, and to a lesser extent the *Design Manual 26.2* of the Naval Facilities Engineering Command (1982), is the standard for coastal engineering and promulgates, among other things, suggested design methods and parameters for the construction of vertical wave barriers.

Existing equations used to determine the wave transmission past, and wave forces on, wave barriers are believed to be overly conservative. Specifically, it is believed that the method of predicting wave transmission as developed by Wiegel (1960) over-estimates wave transmission for most conditions of interest. The Miche-Rundgren method for computing force, as outlined in *NAVFAC DM 26.2,* assumes the worst-case condition of a wave crest on the incident side of the barrier and a wave trough on the other. This maximizes the difference in wave pressure across the barrier and is an unrealistic assumption. The predicted forces from this method are greater than those that would actually occur, which can result in the over design of these breakwaters. Larger cities such as Seattle can sometimes afford to build these breakwaters. However, the inflated costs of this type of breakwater often prevent their use in smaller communities. The Canadian government, for example, has considered the use of this type of breakwater to protect numerous small fishing harbors on the British Columbia coast, but then usually rejected the design due to excessive cost (Wave Barrier Symposium, 1995).

This Trident study was undertaken to improve the theory used in the design of wave

barriers and to generate laboratory data to validate the new theory. This study had four main parts: (1) literature search of experiments and theories in related areas; (2) development of modified theories for wave forces on and wave transmission under a thin wall; (3) regular and irregular wave tests on a thin, rigid vertical breakwater to obtain experimental data; and (4) evaluation of theories based on measured values of wave transmission and wave forces.

The literature search for prior experiments and theories for transmission and forces was conducted in order to gain an idea of the type of testing performed in previous experiments, the theories that were used and/or developed in these tests, real-world applications of these breakwaters, and the construction methods of these breakwaters. Modified theories concerning forces and wave transmission were developed based on Wiegel's (1960) theory and differ mainly as a result of the inclusion of wave reflection in the development of theory. The laboratory data are based on tests conducted in the 120 foot wave/towing tank of the U.S. Naval Academy Hydromechanics Laboratory on a model rigid, thin vertical wave barrier. The regular and irregular tests were conducted to measure wave setup on the structure, the resultant forces on the wall due to wave action, and transmitted wave height and to then compare the regular and irregular results to the modified theories. Particle velocities under the wall and pressures in front of the wall were also recorded for some tests.

BACKGROUND

The primary purpose of a vertical wave barrier is to reflect incident wave energy, thereby creating an acceptable wave climate in the area behind the barrier acceptable for the mooring of small boats. For most breakwaters used in harbor-protection, effectiveness is determined by their reduction of transmitted wave height. This is quantified through the coefficient of transmission, K_t, which is equal to transmitted wave height, H_t, divided by incident wave height, H_i.

$$K_t = \frac{H_t}{H_i} \tag{1}$$

The transmission allowed by wave barrier breakwaters is variable and is primarily a function of wave length, water depth, and breakwater penetration. Wave forces, on the other hand, depend predominantly on wave reflection and also display a much stronger dependence on wave height than is shown by wave transmission.

Wave period is an important factor because wave length is dependent solely on wave period. In deep water, the wave length, L (Figure 5), is given by the relationship

$$L = \frac{gT^2}{2\pi} \tag{2}$$

where g is the force of gravity, and T is the wave period. It is wave length, not wave height, that has a primary influence on transmission. Seemingly contrary to common sense, the

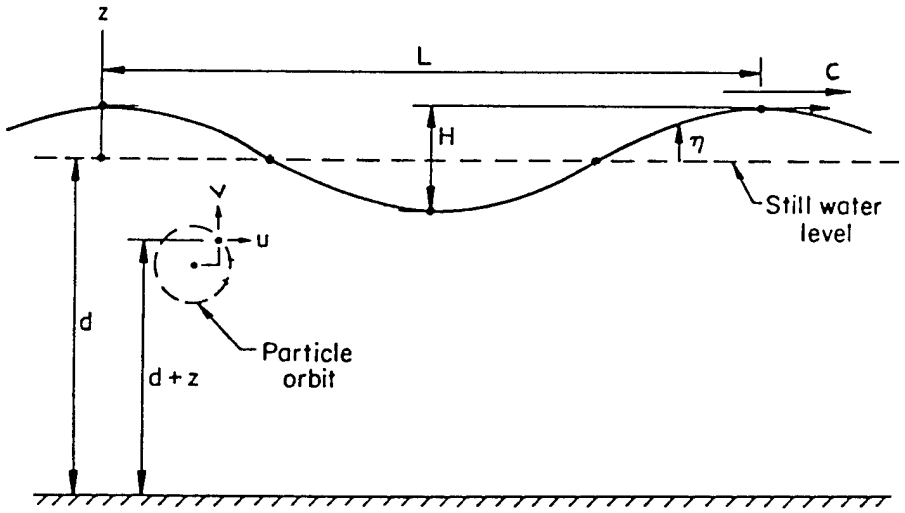

Figure 5. Diagram of basic wave notation. Sorenson (1993), pp. 8.

amount of wave energy present has no influence on the coefficient of transmission. The vertical distribution of this energy is the critical factor, and wave length is what determines the distribution of the energy in a wave. The magnitude of transmission is dependent on how much of this energy is present at a depth that will pass below the vertical wall. The depth to which water particles are affected by a wave is called the "wave base" and is equal to one-half the wave length. Thus, the transmission coefficient depends primarily on wall penetration relative to wave base, or relative to one-half of the wavelength. For instance, if the bottom of the wall is below the wave base, there will be no wave transmission.

Water depth influences transmission indirectly by influencing wave length in intermediate and shallow water. As stated above, in deep water wave length is dependent only on period. The definition of "deep water" is relative to water depth and applies whenever the depth is greater than or equal to one-half of the wavelength. As long as the wave base does not touch the sea floor, the wave is in deep water. As the wave base begins to come into increasingly greater contact with the sea floor, the wave length is shortened due to the constraint of particle orbits by the sea floor. This shortening follows the equation

$$L = \frac{gT^2}{2\pi}\tanh kd \qquad \textbf{(3)}$$

where $k = 2\pi/L$ and d is the water depth. This equation is applicable in intermediate water, which extends from depths of L/2 to L/20. Finally, as the wave approaches the shoreline and passes a depth of L/20, it enters shallow water and its length is given by

$$L = T\sqrt{gd} \tag{4}$$

Wall penetration (w) is a crucial factor because it can be adjusted by the designer to control the amount of transmission. Past wave records can be analyzed and the data can then be used to predict the wave periods that the vertical wall breakwater will be subject to. The maximum expected wave periods and therefore wave lengths will have to be considered in designing a vertical wave barrier. If a designer wishes to eliminate all wave action behind the barrier, he must only extend the barrier past the wave base. Normally, however, a certain amount of transmitted energy is permitted in the design in the interest of monetary savings, and this makes the determination of the wall penetration a critical, site-specific, and potentially risky decision. As will be shown, reducing wave barrier penetration leads to a reduction in the wave force on the barrier, although this is at the expense of increased wave transmission.

Wave reflection also plays an important role in determining wave forces. When a wave reflects from a vertical wall, it no longer appears to propagate or move in the direction of travel. Rather, the wave seems to be fixed in place with the water surface moving only up and down. This condition is referred to as a "standing wave." By summing the equations for water particle motion and crest elevation of the incident and reflected waves, the motion of the water particles and wave crest elevation in a standing wave can be determined. It must be remembered that the reflected wave is moving in the opposite direction of the incident wave and thus constructive and destructive interference will occur when these

waves are superimposed. Thus, in a standing wave, at the wall location, or antinode, all water particle motion is vertical and the surface elevation is equal to the sum of incident and reflected wave heights. The maximum crest amplitude at the wall is equal to $(H_i + H_r)/2$ and is repeated every one-half wave length away from the wall, as shown in Figure 6. At the antinode, or trough, particle motion is horizontal and the surface elevation is equal to the difference of incident and reflected wave heights, or $(H_i - H_r)/2$.

The coefficient of reflection is a measure of the amount of reflection and is given by the equation

$$K_r = \frac{H_r}{H_i} \tag{5}$$

In a perfectly reflecting wave, this coefficient will equal unity, and reflected height will equal incident height. For vertical wave barriers, reflection will be incomplete and K_r will be less than one since some energy is transmitted under the wall while other energy may, in fact, be dissipated.

Incident wave height is important for two different reasons. First, it has a great influence on determining the amount of energy in a wave, given by the relation

$$E = \frac{1}{8}\rho g H^2 L \tag{6}$$

where ρ denotes the specific gravity of water and H is wave height. Second, if a wave is sufficiently high, a portion of it may pass over the top of the breakwater. This is called

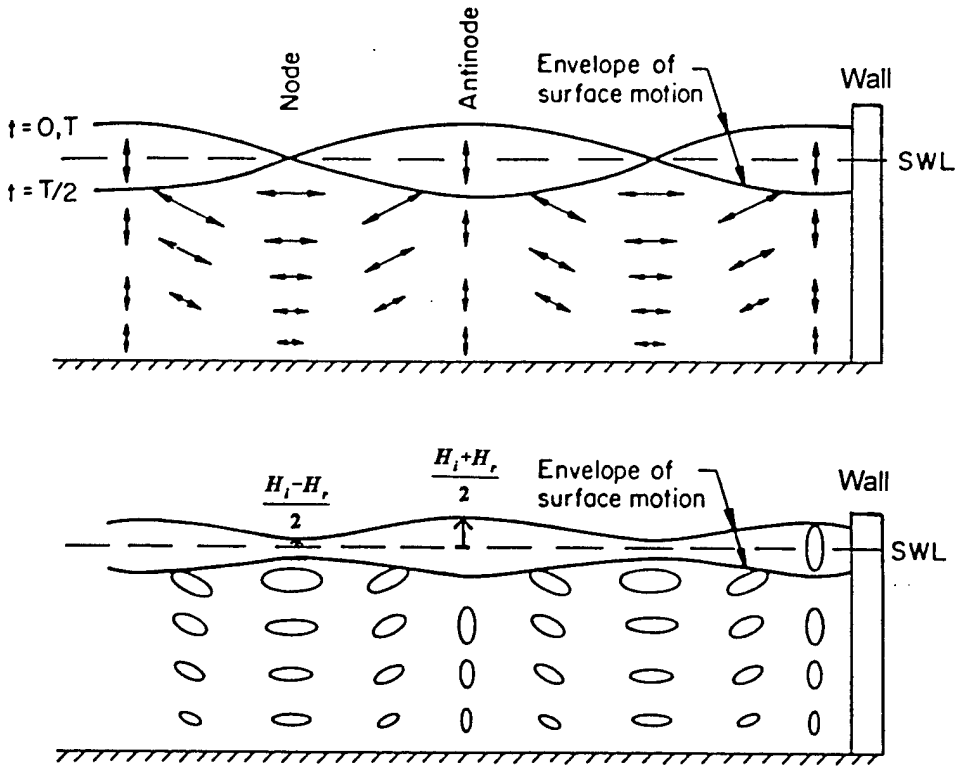

Figure 6. Diagram of standing wave at wall. Sorenson (1993), pp. 26.

overtopping and may result in the transmission of a large amount of energy. Since most wave barriers are designed to be sufficiently high to prevent overtopping, however, conservation of wave energy over a flat bottom requires that all incident wave energy must pass underneath, be reflected, or be dissipated by the barrier. This is shown in the equation

$$E_i = E_t + E_r \tag{7}$$

where E is the energy density and the subscripts I, r, and t refer to the incident, reflected, and transmitted waves respectively. When equation (6) is substituted into equation (7), conservation of energy for partially transmitted, partially reflected waves gives

$$H_i^2 = H_t^2 + H_r^2 \tag{8}$$

and thus

$$1 = K_t^2 + K_r^2 \tag{9}$$

As a wave impacts a full-depth wall, all wave energy must be reflected. The amplitude of the reflected wave will add to the amplitude of the incident wave when a wave crest is at the wall. This increased wave height will increase the dynamic pressure on the wall. The force on a wall due to a perfect standing wave is then given by the equation

$$f = \frac{\rho g d^2}{2} + \frac{\rho g H_i}{k} \tanh kd + \frac{\rho g H_i^2}{2} \quad \textbf{(10)}$$

where f is force per unit length, the first term computes the hydrostatic pressure on the wall and the second term computes the force due to dynamic pressures of the wave acting below the still water level. The third term computes the force due to dynamic pressure in the crest of the wave above the still water level. If this equation is applied to a wall with water on both sides, the first term will be balanced by the hydrostatic pressure from water on the other side of the wall. The large force from the first term that results from dynamic pressure below the still water level is called a "first order force." The smaller dynamic pressure on the wall due to the crest of the wave is the source of the "second order force."

LITERATURE REVIEW

WAVE TRANSMISSION

As previously mentioned, studies on vertical wave barriers have been limited. Professor Robert Wiegel of the University of California at Berkeley is responsible for most of the theory that has been developed for application to vertical wall breakwaters. Wiegel (1960) used two different theories to predict the ratio of transmitted to incident wave heights, or reflection coefficient. A deep water theory was developed by Ursell in 1947 and states that

$$K_t = \frac{H_t}{H_i} = \frac{K_1(2\pi w/L)}{\sqrt{\pi^2 I_1^2(2\pi w/L)+K_1^2(2\pi w/L)}} \qquad \textbf{(11)}$$

where w is the wall penetration and K_1 $(2\pi w/L)$ and $_1I$ $(2\pi w/L)$ are modified Bessel functions. Wiegel then developed a theory for wave transmission valid in all depths through the use and manipulation of power transmission theory. Starting with the equations for dynamic pressure and water particle velocity, Wiegel determined the power transmitted past a vertical plane based on linear wave theory. After some mathematical manipulation of terms, he determined that

$$K_t = \frac{H_t}{H_i} = \sqrt{\frac{2k(d-w) + \sinh(2kd-2kw)}{2kd + \sinh 2kd}} \qquad \textbf{(12)}$$

In laboratory experiments Wiegel determined that the power transmission theory predicted laboratory results more accurately than the deep water theory for small values of barrier penetration. This was verified by Mattson and Cederwall (1976) as shown in Figure 7. Wiegel found the opposite to be true for larger barrier penetrations. He also observed a trend of decreasing transmission with increasing wave steepness. His final conclusion was that wave barriers should be used with caution because they don't significantly prevent wave transmission unless they have a large penetration.

Mattson and Cederwall (1976) performed a series of experiments to measure the coefficient of transmission under various conditions and then compared these measurements to Wiegel theory. Their findings verified Wiegel's conclusion that predictions for transmission varied with barrier penetration. This is shown in Figure 8. They also concluded that Wiegel's theory is relatively inaccurate in extreme cases. Mattson and Cederwall also concluded that transmission is only a function of wall penetration and wavelength. They did this by plotting their experimental coefficients of transmission versus various non-dimensional parameters. Penetration divided by wavelength (w/L) is the only parameter that resulted in reasonable data correlation. Through curve filtering they developed a new equation for the coefficient of transmission, based solely on incident wavelength and wall penetration:

$$K_t = \left[\frac{\cosh 0.5kw}{\cosh kw}\right]^2 \qquad \textbf{(13)}$$

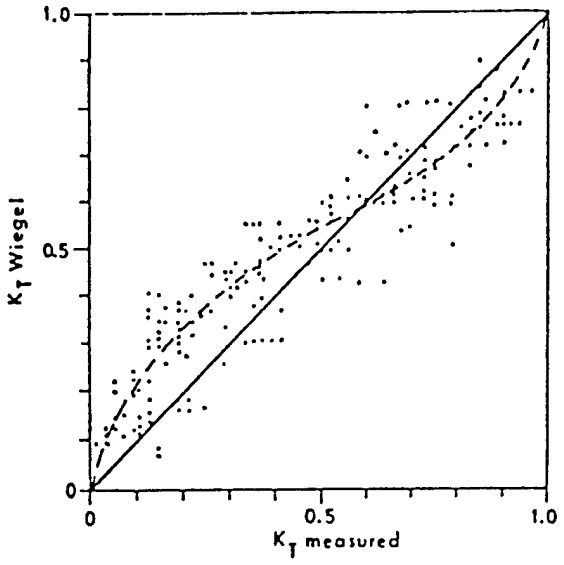

Figure 7. Wiegel theory compared to measured values of K_t, Mattson and Cederwall (1976), pp. 7.

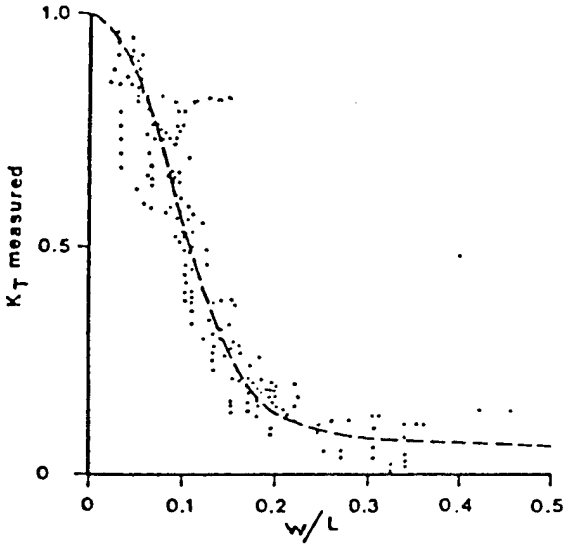

Figure 8. Graph of the dependence of Kt on penetration relative to wave length (w/L), Mattson and Cederwall (1976), pp. 7.

Another interesting finding was that irregular waves appeared to have a greater coefficient of transmission than regular waves. Mattson and Cederwall concluded that deviations from Wiegel theory was most likely the result of energy loss due from vortex formation as water flowed underneath the breakwater. Also, wave reflection from the wall generates non-linear conditions in front of the wall which may invalidate wave linearity assumptions made by Wiegel.

Losada et al (1992) examined the applicability of linear theory to wave interactions with vertical wall breakwaters. An eigenfunction expansion method was applied to obtain theoretical solutions for transmission and reflection coefficients. This paper utilized two assumptions that were adopted in the theoretical development of this Trident project concerning velocity and pressure at the breakwater: Both pressure and velocity were assumed to be constant across the gap underneath the barrier. The numerical analysis demonstrated in this paper created a numerical theory which predicted much larger coefficients of transmission than those from Wiegel. Losada et al also showed that forces on the barrier were a function of barrier penetration as well as water depth and could be computed by vertically integrating the pressure difference across the wall using the equation

$$f(z) = \int_{-w}^{0} (p_2 - p_1) dz \qquad \textbf{(14)}$$

where f is the force on the wall, p_2 is the pressure on the front of the wall, p_1 is the pressure on the back of the wall, and w is the penetration of the wall.

Several papers have been written by engineers at the company of Peratrovich,

Nottingham and Drage, Inc. (PN&D) regarding vertical wall breakwaters. They review the history and development of these breakwaters, describe tests conducted on breakwater models for feasibility studies, and conclude that vertical wall breakwaters are very effective at decreasing wave transmission and perform as designed. One report notes that in the case of a vertical wall breakwater in Garibaldi, Oregon, the structure stood undamaged from storm conditions twice as severe as design conditions (PN&D, Issue #30, undated). It is not clear, however, whether these observations were made regarding incident wave heights or, more likely, the sum of incident and reflected heights.

Gilman and Shaver (1992) reported on tests performed on a model of a PN&D wave barrier. The tests measured wave transmission and loadings in hopes of optimizing designs for proposed wave barrier installations in Seward, Alaska and Seattle, Washington. The model was constructed of epoxy-coated sheets of plywood connected to an aluminum and steel frame which allowed elevation and slope changes of the barrier. Geometric scaling was at a 1:12 ratio with velocities and times scaled according to Froude modeling laws. The model was subjected to regular waves with full-scale periods between three and six seconds and irregular wave trains based on JONSWAP frequency spectra in a full-scale water depth of 18.3 meters. During testing, the barrier limited transmission to 25% when penetration-to-depth ratios were greater than approximately 0.3. Gilman and Shaver (1992) noted that most deep water waves were completely reflected when penetration was greater than 6 meters and that much of the lower-frequency wave energy was reflected in that case as well. They concluded that the tested wave barrier could withstand wave heights of three meters in real life and would therefore be very useful in areas not completely subjected to open-

ocean wave assault.

FORCES ON VERTICAL WAVE BARRIERS

The Army Corps of Engineers's *Shore Protection Manual* (1984) and Naval Facilities Engineering Command *Design Manual 26.2* (1982) contain an extensive analysis of wave forces on vertical walls. Although not specific to wave barriers, the theory is very similar and can be applied to vertical wave barriers with a few simple modifications. The *Shore Protection Manual* (SPM) relies on the aforementioned Miche-Rundgren method of determining non-breaking wave forces (Figure 9). In this method, the height of water at the wall is determined to be equal to the sum of incident and reflected wave heights and can be assumed to be twice the incident wave height with perfect reflection ($K_r = 1$). The water height will oscillate about a point (h_o) above the still water level. This elevation is located midway between the wave crest and wave trough and is greater than zero for nonlinear waves because such waves are asymmetric with crest amplitudes that are greater than trough amplitudes. Wave forces on the wall are determined to be the sum of hydrostatic ($p_h = \rho g d$) and dynamic pressures (Figure 10). The dynamic pressure at the sea floor is given by:

$$p_d = \left(\frac{1 + K_r}{2}\right)\frac{\rho g H_i}{\cosh\left(2\pi d/L\right)} \qquad \textbf{(15)}$$

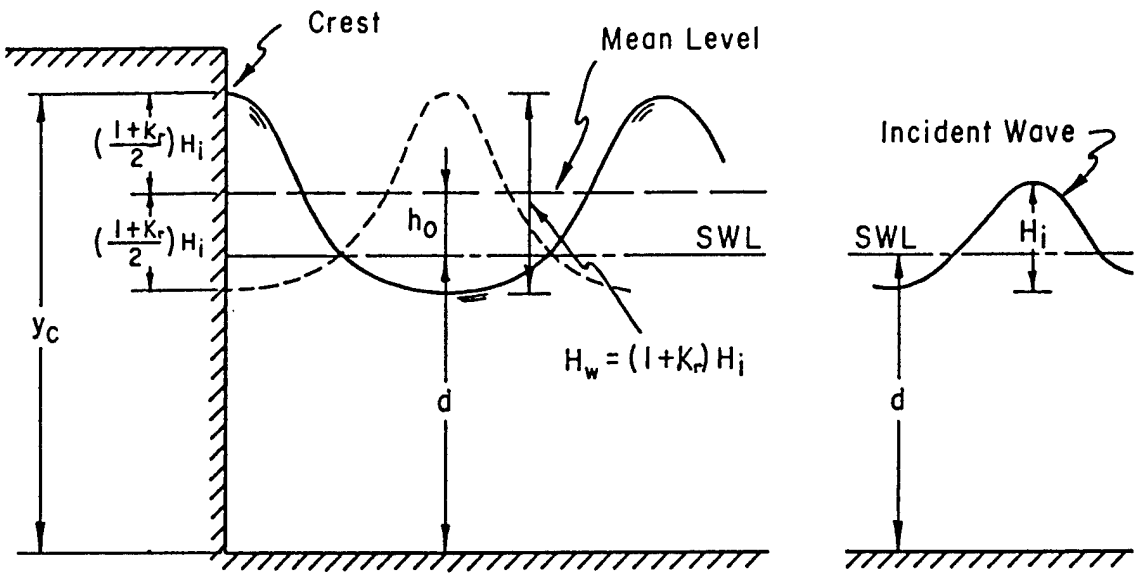

Figure 9. Sketch of terms in Miche-Rundgren method of predicting forces on walls. U.S. Army Corps of Engineers (1984), pp. 7-162.

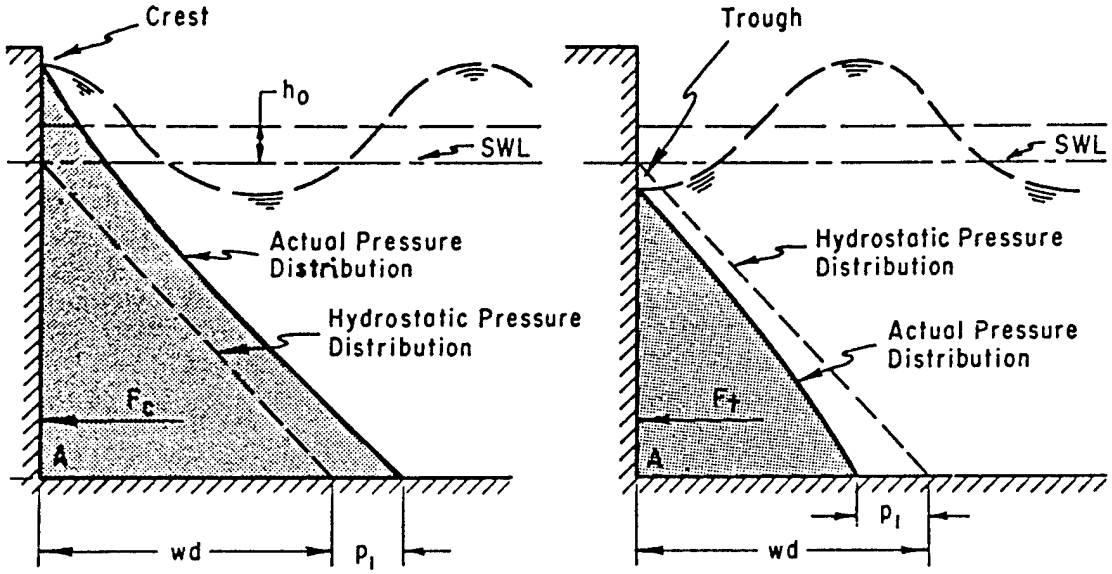

Figure 10. Hydrostatic and dynamic pressures on a wall. U.S. Army Corps of Engineers (1984), pp. 7-163.

When a wave crest is at the wall, the force on the wall per unit width is then approximated by

$$f = \frac{1}{2}(\rho g d + p_d)(d + h_o + H_i) \tag{16}$$

This force is then presented in a dimensionless form given by

$$\frac{f}{\rho g d^2} = \frac{1}{2}\left(1 + \frac{p_d}{\rho g d}\right)\left(1 + \frac{h_o}{d} + \frac{H_i}{d}\right) \tag{17}$$

Similar expressions can be derived for the force when a wave trough is at the wall. Example graphs from the SPM for determining these forces are shown in Figures 11 and 12. These graphs require several secondary calculations and can cause error in force prediction because of the interpolation that is necessary to read data.

The SPM then develops theory and contains an example for the force on a wall built on a rubble foundation. As shown in Figure 13, the distribution of force in this case is extremely similar to that on a vertical wave barrier. The force in this case is shown to be

$$f'' = (1 - r_f) f \tag{18}$$

where r_f is simply a force reduction factor

$$r_f = \frac{d-w}{d}\left(2 - \frac{d-w}{d}\right) \tag{19}$$

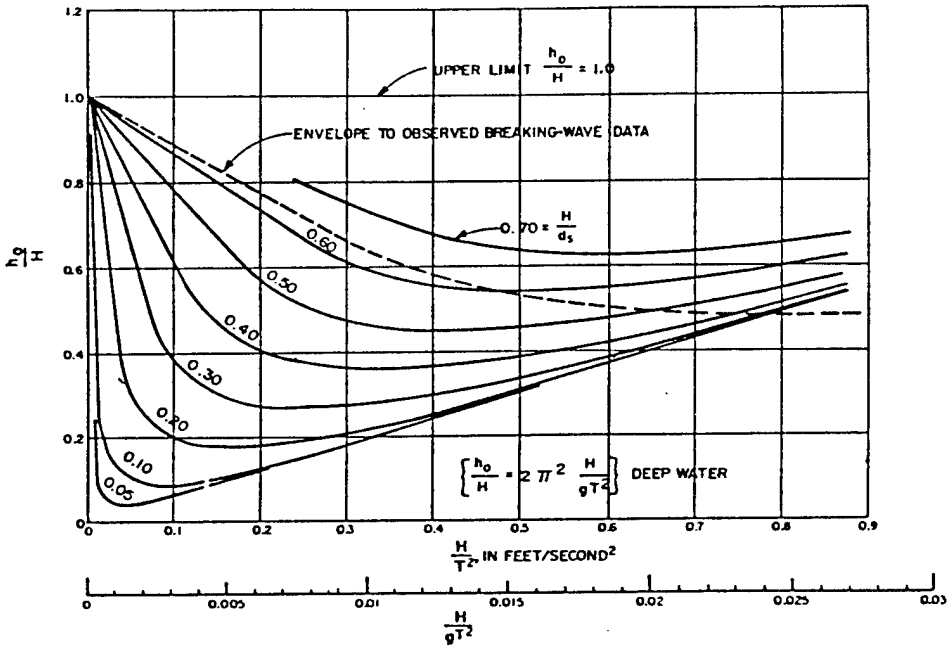

Figure 11. Required figure for force prediction using Miche-Rundgren method. U.S. Army Corps of Engineers (1984), pp. 7-164.

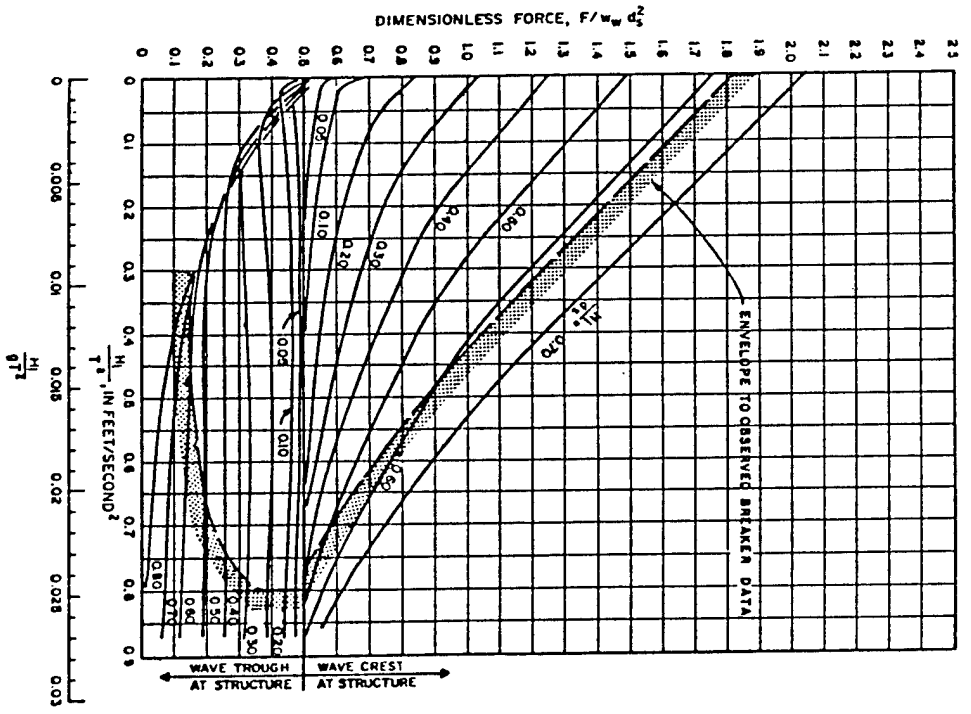

Figure 12. Required figure for force prediction using Miche-Rundgren method. U.S. Army Corps of Engineers (1984), pp. 7-165.

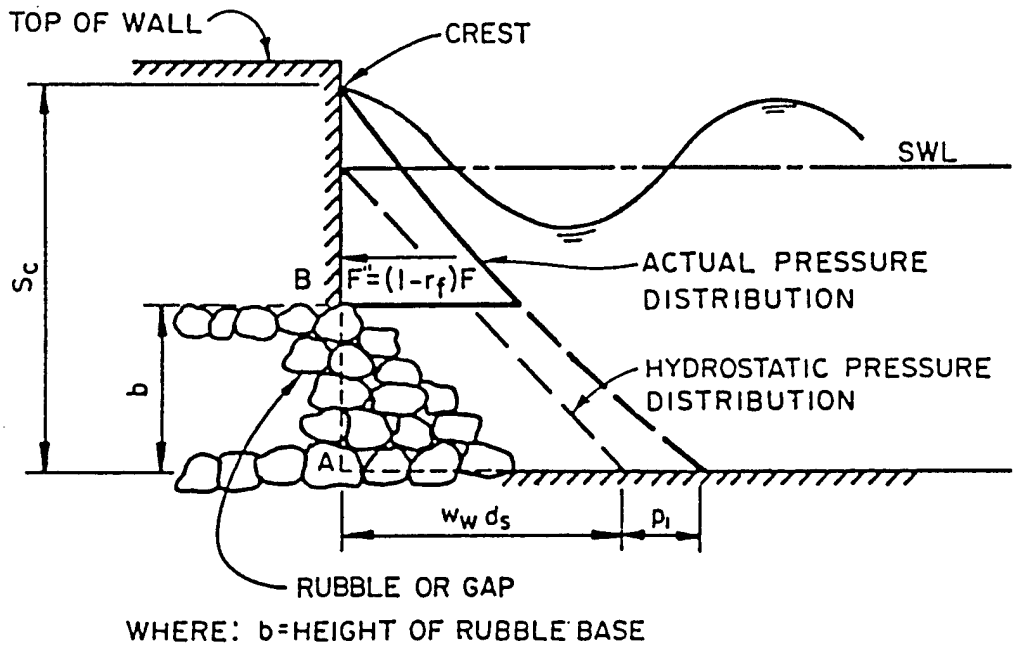

Figure 13. Distribution of force on a wall atop rubble foundation, a case similar to a wave barrier. U.S. Army Corps of Engineers (1984), pp. 7-178.

proportional to the height of the foundation, d - w, divided by the total height of the wall, d.

The NAVFAC Engineering Design Manual (1982) contains an example problem specific to vertical wave barriers. The equations for computing forces on the barrier are the same as those used by the SPM in the rubble foundation example. This example problem and method were used as examples to which to compare project-generated experimental and theoretical data. One critical assumption employed by both the NAVFAC and SPM methods is that a wave crest is on the incident side of the barrier while a wave trough is on the leeward side of the barrier. As noted, this produces the maximum possible pressure difference across the wall and thus the maximum force on the wall. Such an occurrence, however, seems unrealistic and appears to predict unrealistically large forces on a wall. As will be shown in later sections, these forces are indeed unrealistically large, typically twice as large as those measured in laboratory experiments.

RESEARCH OBJECTIVES

Based on the review of existing literature, it was determined that there was a need for additional research in the areas of wave transmission and wave forces. Specifically, this additional research in the area of wave transmission included the development of a modified theory of wave transmission, a comparison of wave transmission data from the laboratory to available theories, and an evaluation of the modified theory for wave transmission when

compared to actual test results. Additional research in the area of wave forces was divided into the same groups as wave transmission: Development of theory, comparison of data to conventional theory, and evaluation of developed theory.

As a result, two main thrusts were developed. The first was to develop a modified theory for wave transmission and wave forces. The second was to then test these theories in the laboratory by comparing experimental data to predictions from the newly developed theories.

THEORY

POWER TRANSMISSION

The modified theory for wave transmission and wave force on a vertical wave barrier is an extension of existing theory as developed by Wiegel (1960). Wiegel proposed that wave transmission could be predicted from the wave power passing under a wave barrier. To make this prediction, Wiegel assumed that there was no energy loss in the system; all energy was either transmitted beneath the barrier or reflected. According to Wiegel, if a vertical power distribution is considered such as in Figure 14, that portion of the wave power that is between the bottom of the barrier and the sea floor will be transmitted. All other incident power will be reflected.

Wave power per unit area is the product of the dynamic pressure (force per unit area) and horizontal particle velocity at any point in a wave. Thus the total power present in a complete wave passing through an imaginary vertical section in two-dimensions is given by the time-averaged product of wave-induced dynamic pressure and particle velocity at this section, integrated from the tank floor to the still-water level. The initial power without any wave barrier present is

$$P = \frac{1}{T} \int_0^T \int_{-d}^0 p\, u\, dz\, dt \qquad \textbf{(20)}$$

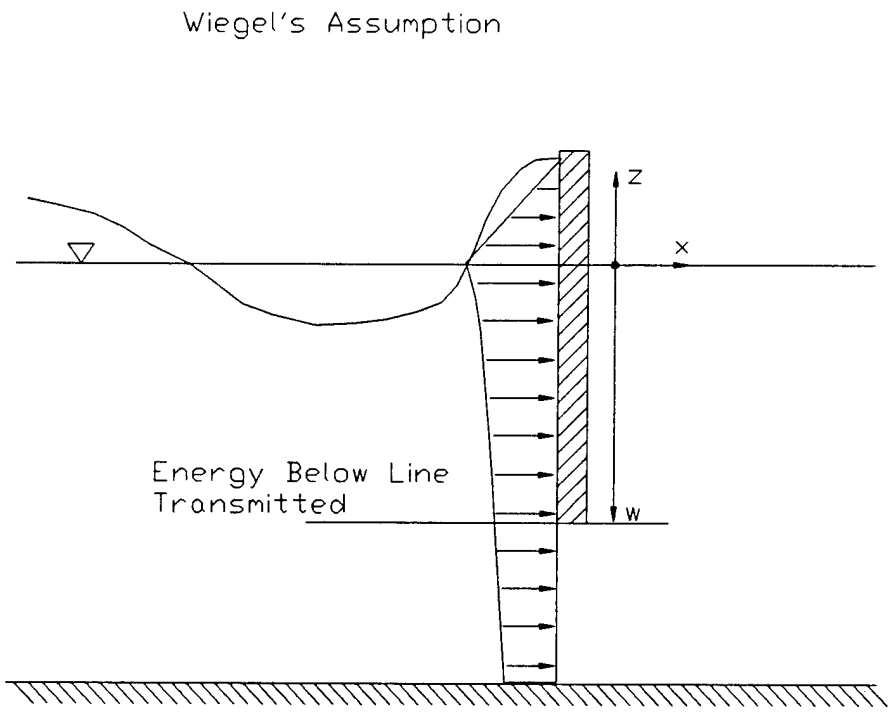

Figure 14. Distribution of wave power approaching a wave barrier.

where P = wave power p = pressure from linear wave theory, and u = the horizontal particle velocity as given in the equations

$$p = \frac{\rho g H}{2} \frac{\cosh k(z+d)}{\cosh kd} \cos(kx - \sigma t) \quad \textbf{(21)}$$

$$u = \frac{\sigma H}{2} \frac{\cosh k(d+z)}{\sinh kd} \cos(kx - \sigma t) \quad \textbf{(22)}$$

where σ is the angular frequency of the wave and is equal to $2\pi/T$. When integrated, (20) yields

$$P = \frac{1}{8} \rho g H^2 C_g \quad \textbf{(22)}$$

where $1/8\rho gH^2$ is the wave energy density and where C_g is the wave group velocity given by

$$C_g = \frac{C}{2} \left(1 + \frac{2kd}{\sinh 2kd}\right) \quad \textbf{(23)}$$

In equation (23), C is the wave celerity and is equal to L/T. Equation (22) is important because it states that wave power in a closed system is constant, independent of time or location, when measured over one complete wave cycle.

WIEGEL THEORY

As stated earlier, according to Wiegel power will only be transmitted across the section of the tank not blocked by the wave barrier. In other words, power will only be transmitted across the gap beneath the bottom of the wall. Therefore, the product of incident wave pressure and velocity (equation 20) need only be integrated between the sea floor (-d) and the bottom of the wall (-w). This generates the following equation for power transmission past a wall:

$$P_t = \frac{1}{T}\int_0^T \int_{-d}^{-w} p_i\, u_i\, dz\, dt \qquad \textbf{(24)}$$

Which, after integration, gives

$$P_t = \frac{1}{8}\rho g H_i^2 C_g \left[\frac{2k(d-w)+\sinh(2kd-2kw)}{2kd+\sinh 2kd}\right] \qquad \textbf{(25)}$$

To find the transmission coefficient, Wiegel reasoned that the power downstream (behind the wall) must equal the power transmitted beneath the wall. Considering a vertical section downstream,

$$P_t = \frac{1}{T}\int_0^T \int_{-d}^{0} p_t\, u_t\, dz\, dt \qquad \textbf{(26)}$$

and the time-averaged transmitted power is given by

$$P_t = \frac{1}{8}\rho g H_t^2 C_g \tag{27}$$

Wiegel determined the coefficient of transmission (as stated earlier in Equation 1) by equating (25) and (27) such that

$$K_t = \frac{H_t}{H_i} = \sqrt{\frac{2k(d-w) + \sinh(2kd-2kw)}{2kd + \sinh 2kd}} \tag{28}$$

MODIFIED TRANSMISSION THEORY

When deriving the power transmission underneath the wave barrier, Wiegel did not consider the effects of reflection upon wave transmission. Consider a lone wave approaching a vertical wave barrier. As the crest of the wave begins to impact the wall, the water level at the wall is rising. As this is happening, part of the wave's energy is transmitted beneath the wall and continues progressing down the tank. The part of the wave's energy that is reflected begins to travel back towards the wave maker. This reflected wave will then interfere, either constructively or destructively, with the incident wave energy that is still approaching the wall.

When the highest point of the wave crest is at the wall, the water level is at its maximum value because the incident and reflected crests constructively interfere. With

perfect reflection the water level at the wall will be equal to twice the incident wave height. Dynamic pressure will also be at its maximum and equal to the sum of incident and reflected pressure. Water particle velocities, however, are not at their maximum value because the incident and reflective wave velocities destructively interfere with each other. The horizontal velocities of the incident wave particles are towards the wall while the particles of the reflected wave are moving away from the wall. Thus when a wave crest is at the wall, pressures are additive (total pressure equals incident **plus** reflected) due to constructive interference and as a result of destructive interference velocities are subtractive (net velocity equals incident **minus** reflected).

The development of a modified theory for wave transmission begins with a modification of the initial power transmission equation to account for reflection, as was already discussed. In the case of a vertical wave barrier, where reflection is not complete, pressures are additive but are not equal to twice the incident pressures and velocities are subtractive but do not completely cancel each other. The transmitted power can then be found by integrating net pressures across the wall and net particle velocities across the gap beneath the barrier such that

$$P_t = \frac{1}{T}\int_0^T \int_{-d}^{-w} (p_i+p_r)(u_i-u_r)\, dz\, dt \qquad (29)$$

Linear theory is used to provide approximations for pressures and velocities. After substitution and integration, the final modified equation for power transmitted under a wall is

$$P_t=\frac{1}{8}C_g\rho g H_i^2(1-K_r^2)[\frac{2k(d-w)+\sinh 2k(d-w)}{2kd+\sinh 2kd}] \quad \textbf{(30)}$$

Some interesting comparisons can be made between this equation and the wave power equation without the effects of reflection (25). From (30) it is evident that any reflection will decrease the modified prediction for net power transmission from that of Wiegel's (equation 25). When there is complete reflection (K_r = 1) there is no power transmission. When there is no wall (penetration w = 0 and hence no reflection), the reflection term as well as the last term (in brackets) go to unity and the original equation for net time-averaged power transmission without a wall (22) remains. Under any conditions where there is a wall, however, the last term associated with wall penetration is less than one, the reflection coefficient is greater than zero, and the power transmitted is less than that predicted by Wiegel.

When the modified wave power equation (30) is equated to transmitted power downstream from the wave barrier in equation (27) , the coefficient of transmission can be determined by simplification to be

$$K_t^2 = (1-K_r^2)[\frac{2k(d-w)+\sinh 2k(d-w)}{2kd+\sinh 2kd} \quad \textbf{(31)}$$

Further simplification is possible if conservation of momentum (mass flow) beneath the wall is assumed. It is recognized that fluid velocities under the barrier are continuous so that

$$u_t = u_i - u_r \tag{32}$$

After substitution of linear wave theory terms for particle velocity and simplification, it is found that

$$K_t = 1 - K_r \tag{33}$$

Finally, combining equations (31) and (33) gives the desired solution for the transmission coefficient

$$K_t = 2\left[1 + \frac{2kd + \sinh 2kd}{2k(d-w) + \sinh 2k(d-w)}\right]^{-1} \tag{34}$$

The assumption of conservation of momentum instead of conservation of energy allows for a loss of energy in the system. Assuming conservation of flow requires a modification of equation (7) to account for the lost energy such that

$$E_i = E_r + E_t + E_{LOSS} \tag{35}$$

If energy loss is considered relative to the incident wave energy and simplifications of the resulting equation are made, a relation for energy loss is obtained such that

$$\frac{E_{LOSS}}{E_i} = 1 - K_r^2 - K_t^2 \tag{36}$$

This equation shows that the maximum energy loss is one-half of the incident energy and will occur when the coefficient of transmission equals the coefficient of reflection, which will only happen when $K_r = K_t = 0.5$.

MODIFIED FORCE THEORY

The force on a vertical wave barrier can be determined by the integration of the pressure difference between the front and back of the wall. The front of the wall is subject to the sum of incident and reflected pressures while the rear of the wall is only subjected to transmitted wave pressure. Thus, the net pressure on the wall at any instant in time equals the pressure at the front of the wall minus the pressure at the back of the wall or $p_i + p_r - p_t$. When these pressures are to be integrated over the height of the wall, thereby yielding force per unit width on the wall, the equation becomes

$$f = \int_{-w}^{0} (p_i + p_r - p_t)\, dz \qquad \textbf{(37)}$$

When this equation is integrated, accounting for a 90 degree phase shift between the incident and transmitted waves, it is found that

$$= \frac{\rho g H_i}{2k}(\cos \sigma t\,(1+K_r) - \sin \sigma t\,(K_t))\frac{[\sinh kd - \sinh k(d-w}{\cosh kd} \qquad \textbf{(38)}$$

The

modified theory was initially derived with the assumption that water levels on both sides of the wall would be in phase. This contradicts the 180 degree phase shift assumed in NAVFAC calculations, but was believed to be more reasonable. After the first test results were analyzed, though, it was discovered that there is a 90 degree phase shift in water levels between the front and back of the wave barrier, as shown in Figure 15. Therefore when a wave crest is at the wall, the water level behind the wall will be at approximately the still water level. One-half second later (for a 0.5 Hertz wave such as in Figure 15) the crest will be at the back side of the wall. When the maximum value of the sine-cosine term is used to predict forces, the previous equation can be further simplified using this assumption and through application of equation (33) to give

$$F_{max} = \sqrt{2}\,\rho g H_i \sqrt{2-2K_t+K_t^2}\,\frac{[\sinh kd-\sinh k(d-w)]}{k\cosh kd} \qquad \textbf{(39)}$$

The above equation accounts for the dynamic pressures due to waves, or, when integrated, the first order forces. First order forces are the dominant factor in predicting the total force on the wall. In the free surface region between the still water level and the wave crest, dynamic pressures are assumed to be like hydrostatic pressures: Increasing from $p_d = 0$ at the crest to $p_d = \rho gh$ at the still water level. The difference in these pressures due to the crest can also be integrated across the wave barrier to obtain another expression for force. This second expression for force is called the second order force. This force is not as large as the first order force, but can account for a significant amount of the total force when conditions with large wave heights are examined. The equation

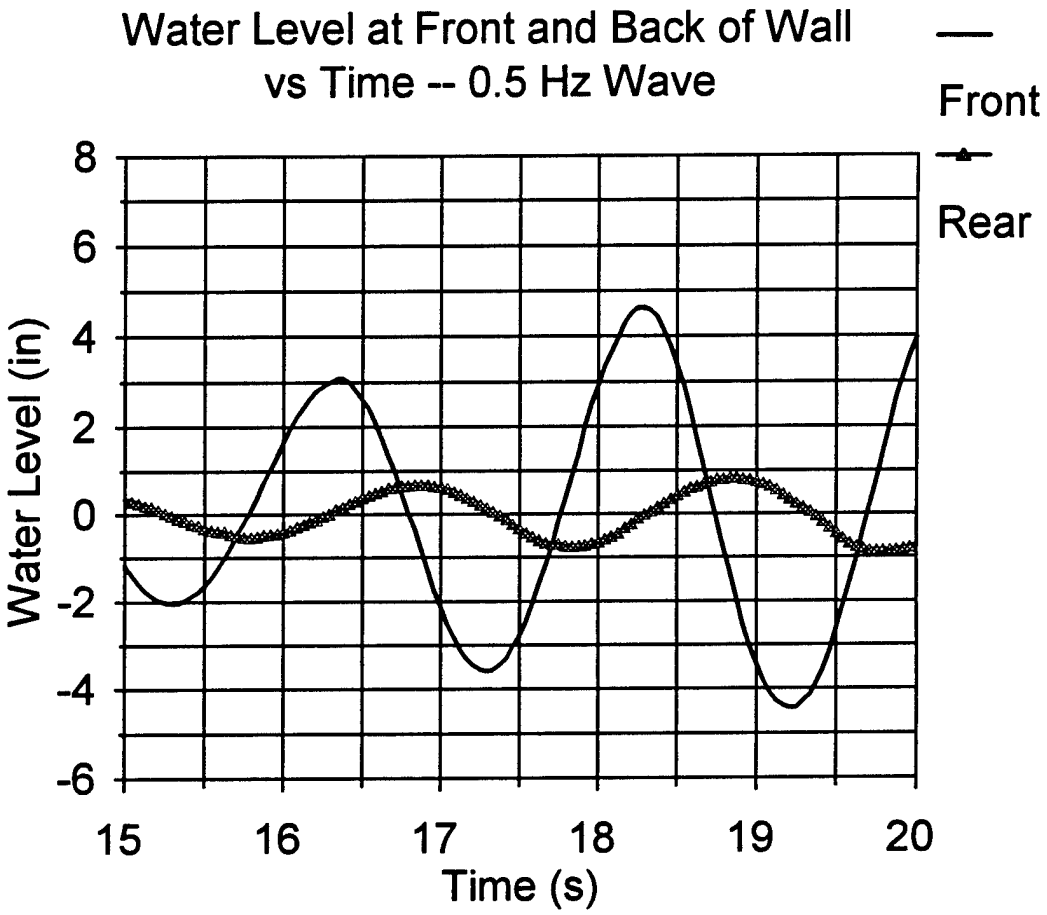

Figure 15. Graph of water level versus time. The 90 degree phase shift between the front and the back of the wall is clearly shown.

for this second order force is

$$f_c = \frac{\rho g(H_i + H_r)^2}{8} \tag{40}$$

where f_c is the adjustment for the crest at the front of the wall and H_w is the water height at the wall. If this adjustment is simplified using equation (33) and added to equation (39) the final modified equation for the maximum dynamic force on a vertical wave barrier is

$$f = \frac{\sqrt{2}\rho g H_i}{k}\sqrt{2-2K_t+K_t^2}\,\frac{[\sinh kd-\sinh k(d-w)]}{\cosh kd} + \frac{\rho g H_i^2\,(2-K_t)}{8} \tag{41}$$

This is a very important equation because it specifies which wave and environmental characteristics determine the force on a vertical wave barrier. From this equation it is apparent that force depends on wave amplitude, wave length, water depth, and wall penetration. Since wave length is in fact determined by wave period and water depth, a functional dependence on wave period is also indicated. One key feature of equation (41) is that force depends on K_t as calculated from equation (34). This presents a challenging cost-benefit analysis problem because while the designer of a wave barrier may seek to minimize wave transmission past a wave barrier into a harbor, this can only be achieved at the expense of larger forces on the barrier. Larger forces then require the construction of a larger, stronger, more expensive breakwater that can withstand these increased forces.

EXPERIMENTAL SETUP

GENERAL SETUP

Testing of the laboratory model was conducted in the United States Naval Academy Hydromechanics Laboratory's 120-foot wave/towing tank. Overall tank dimensions are 120 feet in length, 8 feet in width, and 5 feet in depth (Figure 16). The tank is fabricated from concrete except for a 25 foot segment from 40 to 65 feet (measured from the wave maker) where the starboard tank wall is constructed of glass viewing windows. A dual-flap type wave maker is used to generate regular and random waves with frequencies between 0.2 and 1.3 Hz and heights up to approximately 8 inches. These waves are then dissipated at the other end of the tank by a sloped beach consisting of lattice bundles of fiberglass rods and stainless steel connectors.

The model vertical wave barrier was placed a little more than 60 feet from the wave maker and was thus slightly closer to the beach than the wave maker because the presence of the glass wall section precluded the mounting of the wall at the exact midpoint of the tank. This allowed valid data to be taken for 15 to 30 seconds, depending on the generated wave, before waves reflected from the beach end of the tank returned to the wall, thus contaminating the data. For tests with regular waves, incident waves were measured with a gage 15 feet from the wave maker. Transmitted waves were measured with a gage 75 feet from the wave maker, or 15 feet behind the barrier. Water levels at the barrier were measured using one wave gage one inch in front of the

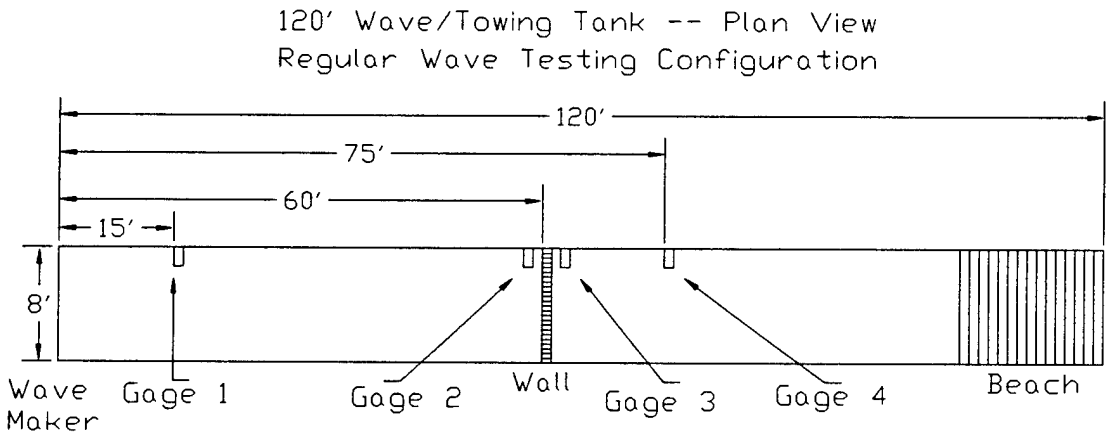

Figure 16. Plan view of wave/towing tank for regular wave setup.

barrier and another gage two inches behind the barrier. The incident and transmitted wave gages were resistance wire probes while those against the wall were capacitance probes. Additionally, a sonic wave probe was mounted on a carriage that runs above the tank for most of its length. The sonic gage (carriage) began its run above the model and moved in the direction of the wave maker in order to record a water surface profile during the experiment that could be analyzed to determine incident and reflected wave heights.

SCALING LAWS

The entire experiment was modeled on a 1:10 scale in order to produce results that could be transferred to a real-life 50 foot water depth according to geometric scaling. In this case, the modeling of a 50-foot water depth by a 5-foot deep tank resulted in a length ratio of 10 such that

$$L_r = \frac{L_p}{L_m} = 10 \tag{42}$$

where L_r is the length ratio, L_p is the prototype length, and L_m is the model length. Froude scaling is used in this problem as Froude scaling is utilized whenever surface gravity wave motions are to be simulated. The equation for the Froude number is

$$Fr = \frac{U}{\sqrt{gL}} \tag{43}$$

where U is a characteristic velocity, L is a characteristic length, and g is the acceleration of gravity. A model and prototype, or real-life structure, will have the same Froude number when velocity and length, the two variables of a Froude number, are proportionally related to give the same value of Fr. With equal Froude numbers

$$\frac{U_p}{\sqrt{gL_p}} = \frac{U_m}{\sqrt{gL_m}} \tag{44}$$

and with some simplification the velocity ratio is given by

$$U_r = \frac{U_p}{U_m} = \sqrt{\frac{L_p}{L_m}} = \sqrt{L_r} \tag{45}$$

Since velocity is the quotient of length and time, the time ratio can then be given as

$$T_r = \frac{T_p}{T_m} = \frac{L_p}{U_p}\frac{U_m}{L_m} = \sqrt{L_r} \tag{46}$$

In this experiment, the use of a length ratio of 10 resulted in a time ratio of $(10)^{½}$. Therefore a 2.0 second period wave from this experiment corresponds to a wave with a period of $2(10)^{½} = 6.3$ seconds in real life. Laboratory test conditions ranged from 0.9 second period to 2.0 second period waves because, when scaled, these wave periods roughly correspond to real-life periods common to inland waters of the Pacific Northwest. (PN&D, Issue #30, undated)

MODEL CONSTRUCTION

The model wall is constructed of G-10 composite sheets laminated onto a waffle interior framework. The composite sheets are 1/4" thick in front of the wall and 3/8" thick on the rear of the structure, with the thicker sheet placed on the back to increase the stiffness of the wall. The interior waffle pattern is composed of square foam and aluminum bar. The foam runs vertically and horizontally and provides buoyancy and rigidity while three strips of aluminum bar are placed vertically to provide additional rigidity to the wall as well as to allow the mounting of the wall onto a support structure. The wall is free-flooding as a result of holes that were drilled through all horizontal section pieces and as a result prevents an excessive buoyant force from developing when the wall is placed in the wave tank and induces in a slight negative buoyancy overall for the structure.

The wall is mounted to a support structure composed of cross-pieces of aluminum angle and support legs composed of aluminum angle and tubing (Figure 17). The aluminum cross pieces are 3" x 3" angle of 1/4" thickness. The bottom cross-piece is reinforced with a 3/8" aluminum plate bolted to the bottom edge. This plate was added to increase the stiffness of the aluminum angle in order to prevent flexure. There are slots cut in the forward leg of angle to allow mounting of the wall to the angle through the use of 1/4" Allen-head screws put into holes drilled and tapped in the aluminum stiffeners of the wall.

The support frame consists of two cross pieces running across the wave tank,

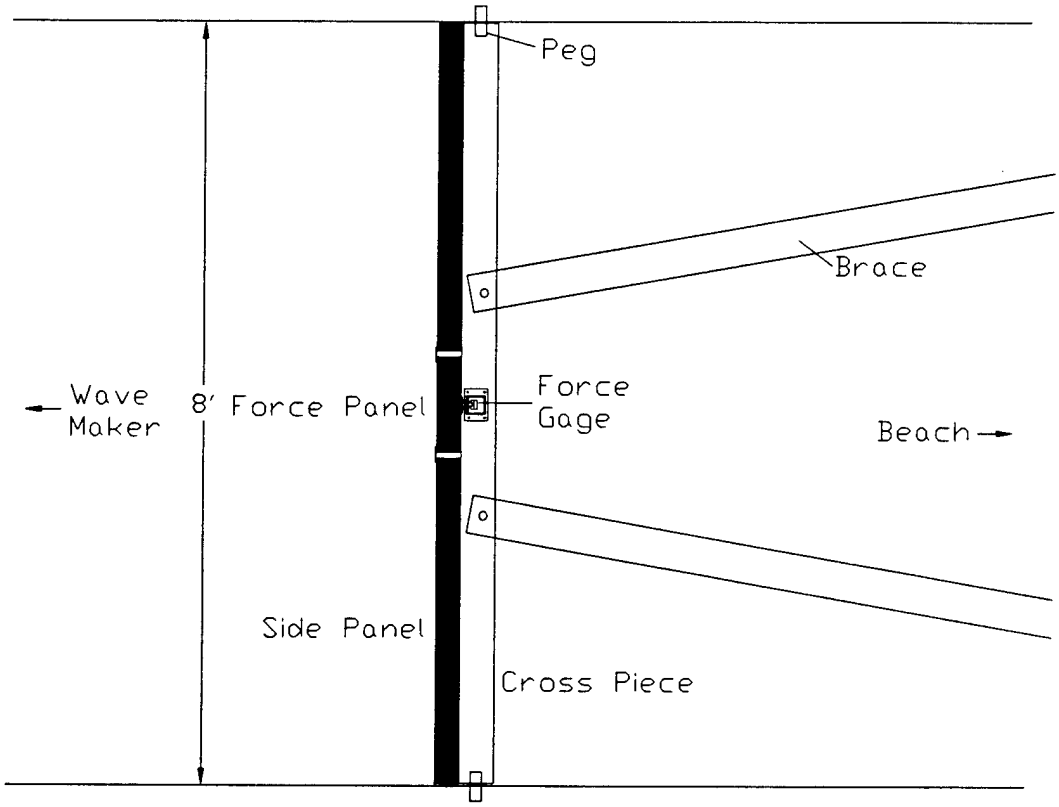

Figure 17. Plan view of model wave barrier.

parallel to the tank floor (Figure 18). They are attached to the tank wall with one inch diameter brass pegs placed through a hole in the end of the cross-pieces into pre-existing holes in the tank walls. The cross-pieces and wall are further reinforced against flexure by the use of structural aluminum members as "tie rods" which run from the cross-pieces to fasteners on the tank wall eight feet behind the model. The bottom members are one inch diameter tubing aluminum, while the top legs are composed of aluminum angle of the same size as the cross-pieces. Tubing was used on the bottom of the wall to decrease interference with the flow behind the wall.

The model wave barrier consists of three distinct sections . The two outside sections are fixed to the support structure by 1/4" Allen-head screws and 5/16" through-bolts. These sections are spaced from the wall by putting each screw through two stacked 1/8" washers before attaching to the wall. The middle section is attached to the support structure only through two pivot-force block connections (Figure 18). These connections allow the measurement of force in the direction of wave propagation.

Rows of holes were drilled in the wall at six inch intervals to allow movement vertically without necessitating a movement of the support structure. It was originally intended to move the wall in the tank by removing the connecting screws, repositioning the wall, and fastening it to the supports once again. However, due to extra hardware used for spacing and reinforcement and the general awkwardness of wall, it soon became readily apparent that this method would be too time consuming to use. After some consideration, the wall was repositioned by removing the rear reinforcing legs and the brass pegs that attached the model to the tank walls. The whole wall was then elevated

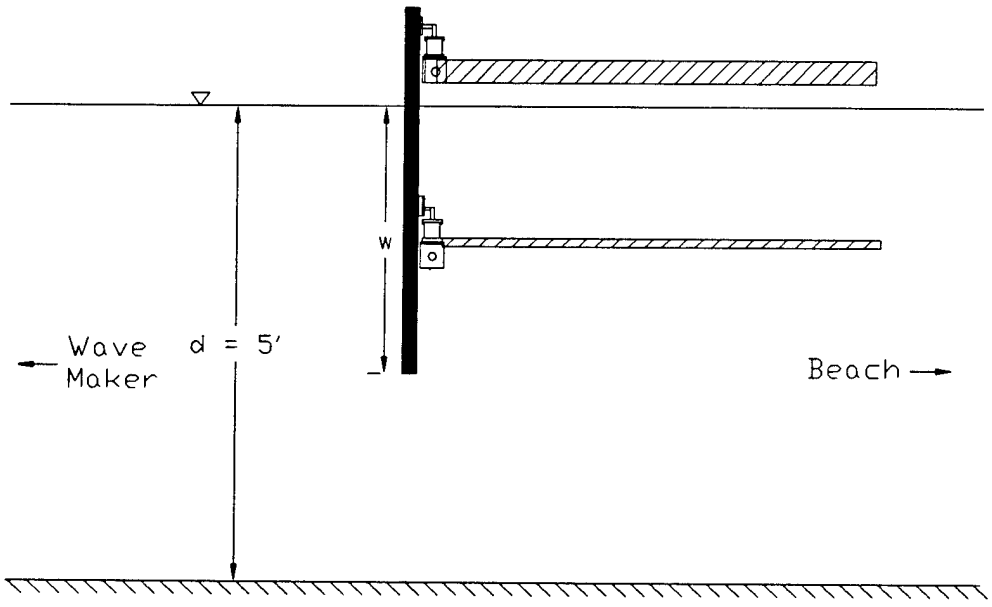

Figure 18. Side view of model wave barrier.

or lowered and the pegs were reinserted in the bottom cross-piece. The top cross-piece was then removed and reattached at its original level at the top of the tank wall. Finally, the reinforcing legs were reattached.

The fine tolerances required in the construction of this model, especially due to the use of two force gages, made construction difficult and time-consuming. Use of a single force gage to measure wave forces by suspending the center panel in cantilever-fashion would have greatly simplified design and assembly. This would have precluded possible determination of the center of pressure or of wave-induced moments on the wall, however.

EXPERIMENTAL CONDITIONS

The first part of the experiment involved the creation of regular waves of fixed frequency and wave steepness in order to test the modified theory for wave transmission and resultant force. Waves with frequencies of 0.5, 0.7, 0.9, and 1.1 Hertz were generated at wave steepnesses of 1/40, 1/20, and 1/15 where steepness is equal to wave height divided by wave length = H/L. The use of fixed slopes instead of fixed wave heights as a testing variable was the result of the observed dependence of the dimensionless wave force, and in particular non-linear wave forces, on the ratio of wave height to wave length (H/L) as shown in the modified theory. All tests were conducted in a water depth of five feet but with three different wall penetrations of 3.0, 2.5, and 2.0

feet. In this first part, waves were measured at 15 feet and 85 feet from the wave maker as well as the front and back of the wall (Figure 16). In addition, the forces on the top and bottom force gages were recorded. Data were recorded for a 30 second duration using a sampling frequency of 24 Hertz.

The goal of the second phase of testing was to measure fluid velocities beneath and in front of the wall in a grid pattern, as shown in Figure 19. This was accomplished with the aid of an acoustic Doppler velocimeter (ADV) manufactured by Sontek, Inc. of San Diego, California (Figure 20). This device emits sonic waves which are reflected by particles in the water. The ADV then measures the Doppler shift of its emitted waves and can determine particle velocities. A special rig was created which allowed the probe to be mounted parallel to the tank bottom, thereby minimally interfering with fluid flow. Additionally, this rig allowed for precise alteration of the probe's position, which was essential for the second part of this testing phase. A 0.5 Hertz, 1/40 steepness wave was generated for this part of the experiment.

The third and final phase of testing studied the effects of random waves on the wall. A computer program was used to generate the random waves in this phase. The program requested the entry of a desired spectrum shape, spectrum width, modal (peak) period, significant height, and number of frames and then proceeded to generate a model spectrum by superimposing sinusoidal waves of different frequencies and amplitudes in order to approximate a spectral shape. This spectrum could then be created in the wave tank, analyzed by the computer, and input into the wave maker after being adjusted to create a more accurately distributed spectrum.

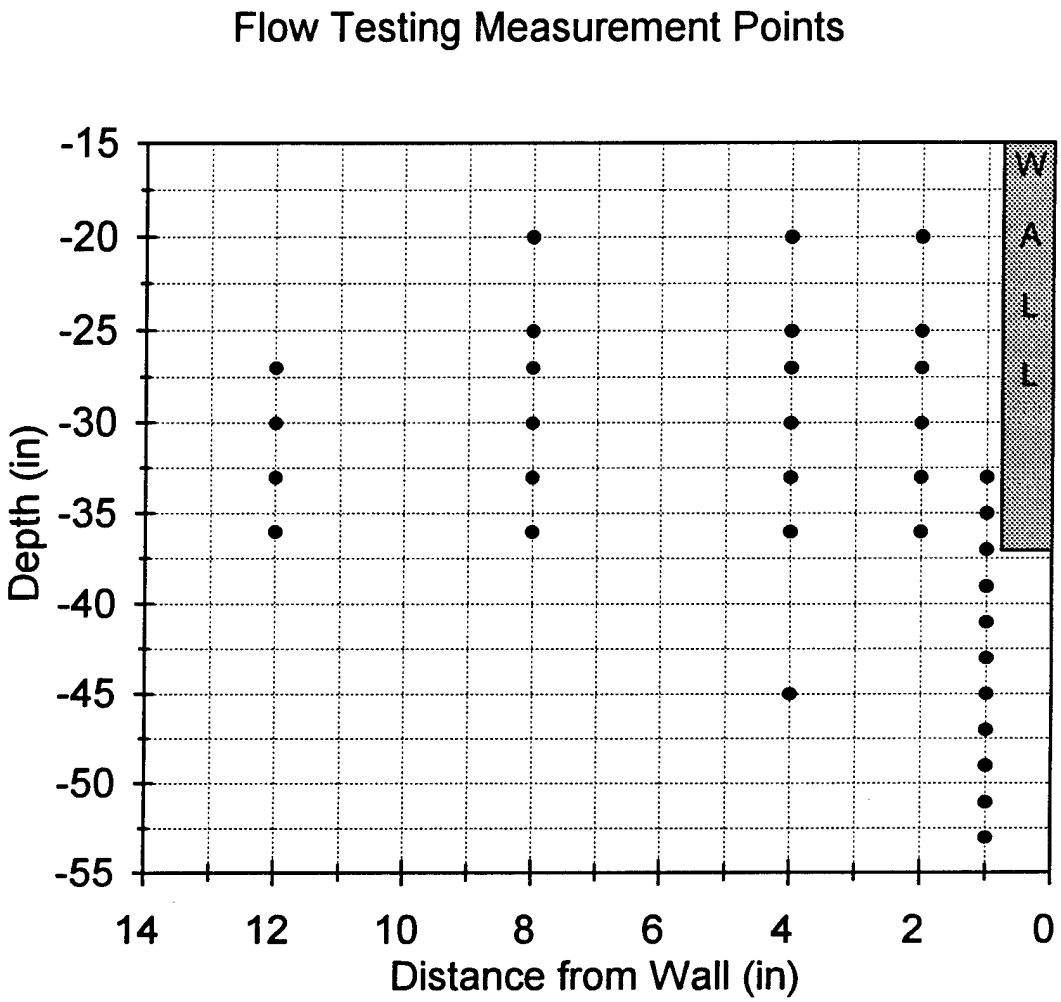

Figure 19. Map of flow test locations under and around model.

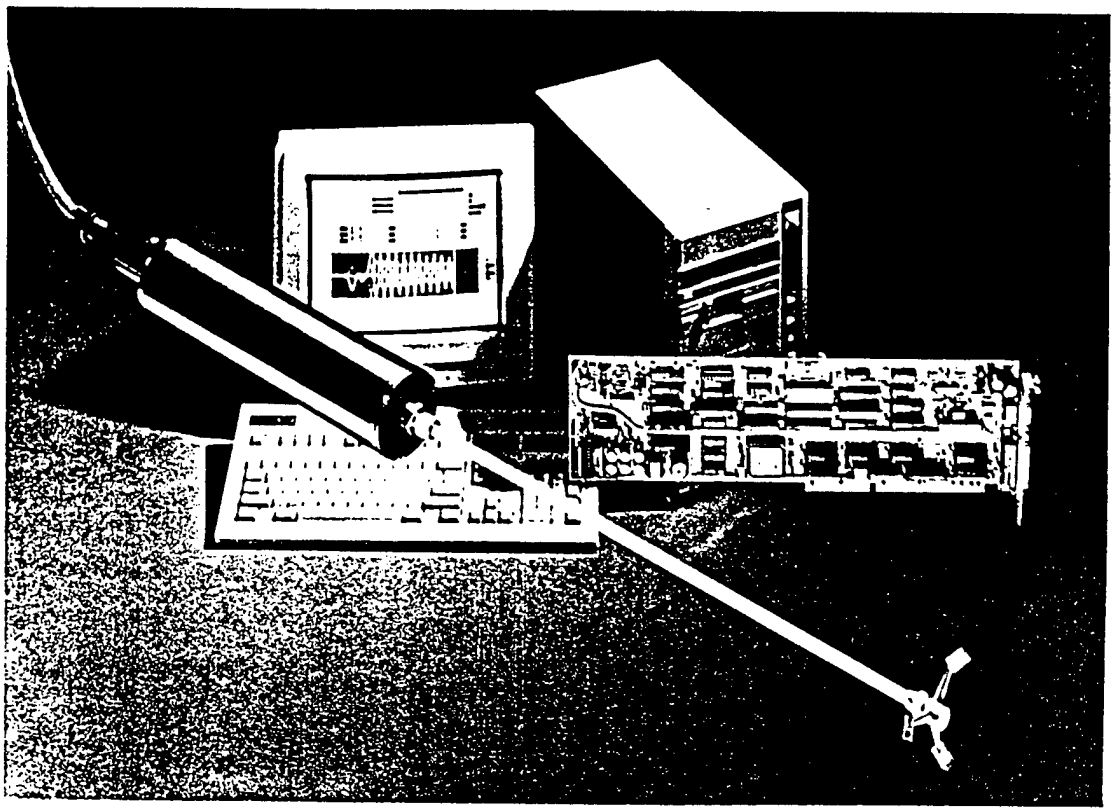

Figure 20. Photo of an Acoustic Doppler Velocimeter.

This program was used to create wave records 60 seconds in length, of 0.5 and 0.7 Hertz modal frequency, with a JONSWAP spectral form having a spectral width of 3.3. The JONSWAP spectral equation is given on page 138 of Sorenson (1993). The significant height, H_s, is a measure of the wave height of the 1/3 largest waves of a spectrum. A significant wave height was chosen that produced a wave steepness $H_s/L = 1/40$. The significant wave height was therefore 5.7 inches for a 0.5 Hertz peak frequency and 3.1 inches for the 0.7 Hertz peak period. Five 60-second time series were created for each modal frequency thus subjecting the model to about 100 total waves at 0.5 Hertz and approximately 140 waves at 0.7 Hertz frequency. Additionally, two wall penetrations of 2.5 and 3 feet were tested. In total, four different experimental conditions were examined.

Force on the wall, incident and transmitted wave heights, and water level at the front and rear of the wall were the variables measured in this section of the experiment. An array of two gages was placed in front of the wall at the 20 foot location in the wave tank and another pair of gages was placed behind the wall at the 80 foot section of the tank. Both pairs were spaced two feet apart for the 0.5 Hertz wave tests and one foot apart for the 0.7 Hertz wave tests. The pair of gages closest to the wave maker was used for an array from which both incident and reflected wave spectra could be resolved while the rear pair of gages permitted the resolution of transmitted spectra as well as the spectra of waves reflected from the beach at the end of the wave tank. Capacitance gages were again used to measure front and rear water levels at the wall. The wall was subjected to the same set of wave spectra at both wall penetrations, requiring the

generation of only two complete spectra: one with a modal frequency of 0.5 Hertz and the other at a modal frequency of 0.7 Hertz.

EXPERIMENTAL RESULTS

Preliminary testing was conducted to evaluate the wall design and functionality of the support frame. Tests that were run yielded valuable ideas for design improvements and indicated that quality data could be obtained with some alterations to the original model design. Full time testing was then initiated and completed and the results are described below.

WAVE TRANSMISSION -- REGULAR WAVES

The experimental setup for this portion of testing was the same as previously described and as is shown in Figure 16. The model was subjected to waves of frequency 0.5, 0.7, 0.9, and 1.1 Hertz and usually three different steepnesses of 1/15, 1/20, and 1/40 at each wave height. Waves with of 0.5 or 0.7 Hertz were not examined at the 1/15 steepness for wall penetrations of 2.5 and 3 feet because laboratory facilities were not capable of handling waves of that magnitude. Wave transmission was determined by recording incident wave height with gage #1 and transmitted wave height with gage #4 (Figure 16). For both incident and transmitted wave records, five complete wave cycles were identified and the five wave crests and troughs were averaged to determine the experimental wave height.

Wave transmission was measured for all testing sequences and then compared

with the modified theory for wave transmission. The results are shown below in Figure 21. This figure compares experimental values of K_t to theoretical values computed using the modified theory for K_t. In Figure 21, data points would fall along a straight line having a 1:1 slope if experimental results perfectly matched theory. Figure 21 indicates that agreement between experimental data and theoretical prediction is generally good with some variations in results for different wave frequencies.

As explained previously, waves with smaller frequencies have longer wave lengths. As a result these waves have a deeper wave base and produce more transmission. Under testing conditions, a 0.5 Hertz wave had a wave length of almost 20 feet and thus a wave base of 10 feet. This was a large enough value to be strongly influenced by changing the penetration of the wall. Note in Figure 21 the three distinct groups of transmission values corresponding to the three tested wall penetrations. The smallest values of transmission for the 0.5 Hertz waves (K_t of approximately 0.3 to 0.4) correspond to the greatest values of wall penetration (w = 3 feet). At 0.5 Hertz, theory tended to underestimate K_t. The error between data and theory, defined as

$$\epsilon = \frac{K_t \exp - K_t pred}{K_t pred} \tag{47}$$

ranged from 5 to 21 % for 0.5 Hertz waves using Wiegel theory or 4 to 23 % using modified theory. The 0.7 Hertz waves had a wavelength of about 10 feet and a wave base of approximately 5 feet. These waves produced some transmission with a K_t between 0.1 and

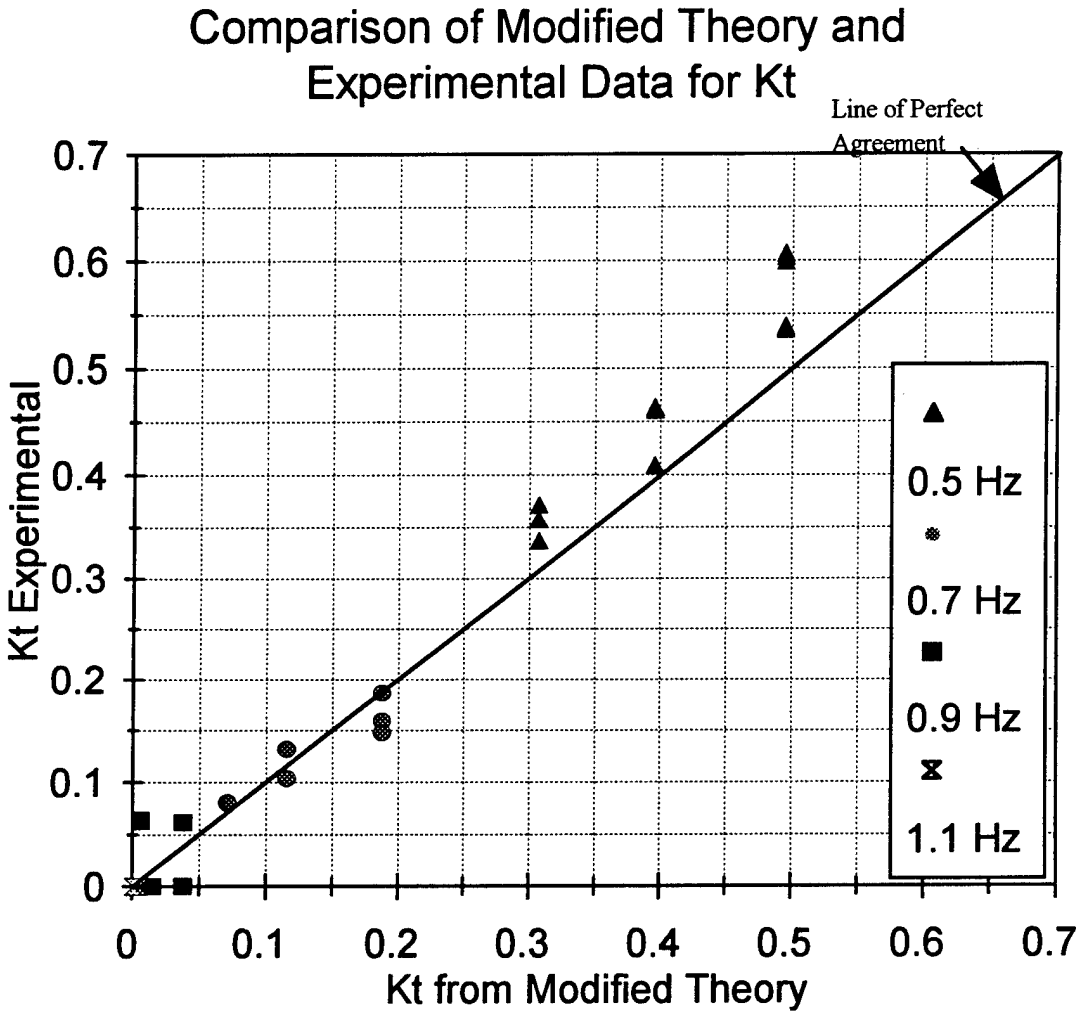

Figure 21. Comparison of modified theory predictions and experimental values of the coefficient of transmission, K_t.

0.2. Theory tended to slightly overestimate transmission for 0.7 Hertz waves but was more accurate overall. Modified theory had an error of 1 to 22% while Wiegel error ranged from 42 to 58%.

Little useful data was obtained from the 0.9 and 1.1 Hertz waves. The 0.9 Hertz waves were approximately 6 feet long and thus were nearly completely reflected by the wave barrier. Scatter in the data is greatest at this frequency because predicted and actual values of wave transmission were so small. Additionally, random noise and inherent error in the system prevented accurate measuring of the extremely small transmitted wave heights. The cluster of 1.1 Hz points at the origin is the result of these waves being nearly perfectly reflected by the test model at all tested penetrations. These data series served mainly as a check in wave interaction with an effectively "full depth" wall since little or no energy from these waves passed beneath the wave barrier.

The results of comparing experimental data from this project with prediction from Wiegel (1960) theory is shown in Figure 22. For most test conditions, Wiegel's theory predicts much larger coefficients of transmission than are actually observed. These results agree with an observation by Mattson and Cederwall (1976) which says, "...Wiegel's equation tends to give too large values of K_t in the interval of interest where $K_t \leq 0.6$." When considered over the tested range, the difference between these two methods is significant, ranging from 15 to greater than 200 %. As a result of the comparisons between Figures 21 and 22, it may be concluded that the modified theory provides a much better prediction of wave transmission than the Wiegel (1960) theory.

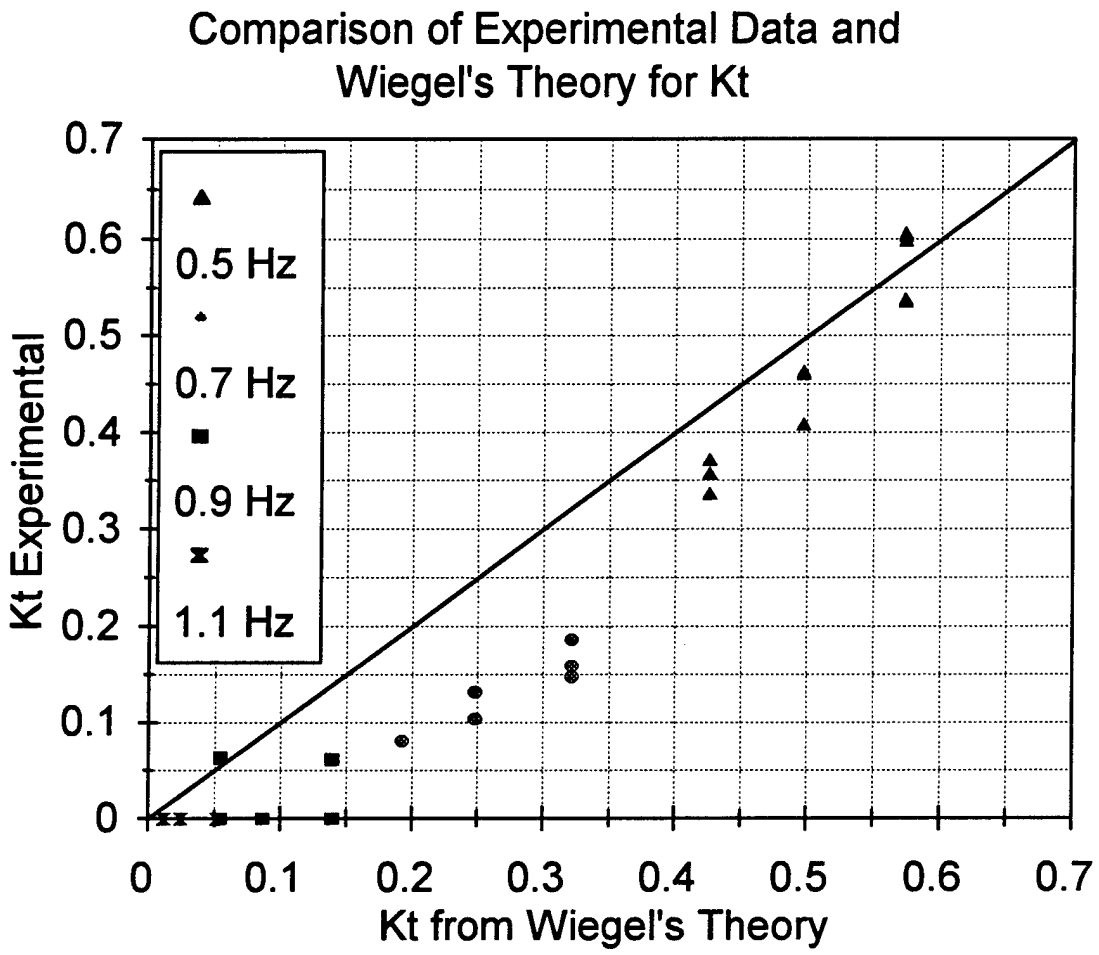

Figure 22. A comparison of Wiegel's theoretical predictions and experimental values of the coefficient of transmission, K_t.

WAVE TRANSMISSION -- IRREGULAR WAVES

Experimental setup for random wave testing is shown in Figure 23. The pairs of gages at 20 feet and 80 feet were separated by 2 feet for waves at 0.5 Hertz peak frequencies and were separated by 1 foot for 0.7 Hertz waves, as explained earlier. Testing was performed at modal (peak) frequencies of 0.5 and 0.7 Hertz and at penetrations of 2 and 2.5 feet. Five 60 second test runs were made at each combination of penetration and peak frequency for a total of 20 data runs involving random waves. Data were taken from six wave gages and two force gages. The wave gages were grouped in pairs with a pair at 20 feet, a pair at the wall (one inch in front of and two inches behind), and the third pair at 80 feet. Both gages at the wall and one of each extreme pair of gages were capacitance gages while the remaining two gages, one of each extreme pair, were resistance-type gages.

Wave heights could not be measured in the same way for irregular wave tests as in regular wave tests. An irregular wave pattern is the result of the random superposition of sine curves at various frequencies and amplitudes. Waves of different frequencies move at different velocities, thus an irregular wave pattern is the result of superposition of many different waves. This superposition prevents the direct measurement of an individual wave's height and thus requires an alternative analysis technique. In addition, reflected waves also travel in a different direction and further complicate wave height measurement. To overcome these difficulties, a method developed by Goda and Suzuki

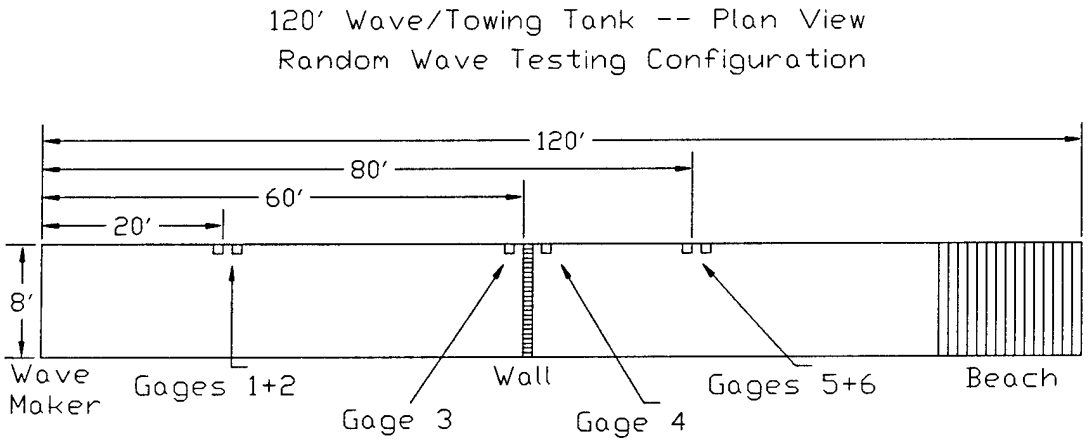

Figure 23. Plan view of wave/towing tank. Setup for random wave data collection shown.

(1976) was utilized in this project for irregular wave analysis. This method involves the numerical analysis of signals obtained from a pair of wave gages in close proximity to each other. The raw data is first analyzed using a Fourier Transform. This transform will calculate the Fourier coefficients A and B at each gage for each frequency in the wave spectrum. These coefficients contain information regarding the amplitude and phase of waves in the spectrum and, when known at two locations, they can be used to separate the incident and reflected waves. Goda and Suzuki (1976) developed a method that allows the prediction of incident and reflected wave amplitudes at each of the wave frequencies from the Fourier coefficients (Figure 24). After the incident and reflected coefficients have been determined, further numerical analysis can then be used to calculate incident and reflected significant wave heights (average of 1/3 largest waves or 4 times the standard deviation of the water surface), which are in turn used to calculate the coefficient of reflection, K_r.

After the random wave data was analyzed using the above procedure, average values of experimental wave transmission (averaged for all five 60 second test runs) were compared to theoretical values predicted using the modal (peak) frequency of the irregular wave spectrum. The results of this comparison are shown in Figure 25. The 0.5 Hertz waves show fairly good correlation with theory. They have the same slope as the line of theoretical prediction but fall below this line. This is because these results are not for a pure wave of a single frequency but rather a wave spectrum that consists of frequencies ranging from approximately 0.4 to 1.0 Hertz. The 0.5 Hertz waves in the spectrum may be reasonably expected to follow theoretical predictions, but the

Further, we suppose that the surface elevations are recorded at two adjacent stations of x_1 and $x_2 = x_1 + \Delta\ell$. The observed profiles of composite waves will be

$$\left.\begin{aligned} \eta_1 &= (\eta_I + \eta_R)_{x=x_1} = A_1\cos\sigma t + B_1\sin\sigma t, \\ \eta_2 &= (\eta_I + \eta_R)_{x=x_2} = A_2\cos\sigma t + B_2\sin\sigma t, \end{aligned}\right\} \tag{2}$$

where,

$$\left.\begin{aligned} A_1 &= a_I\cos\phi_I + a_R\cos\phi_R, \\ B_1 &= a_I\sin\phi_I - a_R\sin\phi_R, \\ A_2 &= a_I\cos(k\Delta\ell + \phi_I) + a_R\cos(k\Delta\ell + \phi_R), \\ B_2 &= a_I\sin(k\Delta\ell + \phi_I) - a_R\sin(k\Delta\ell + \phi_R), \end{aligned}\right\} \tag{3}$$

$$\left.\begin{aligned} \phi_I &= kx_1 + \varepsilon_I, \\ \phi_R &= kx_1 + \varepsilon_R. \end{aligned}\right\} \tag{4}$$

Equation 3 can be solved to yield the estimate of

$$\left.\begin{aligned} a_I &= \frac{1}{2|\sin k\Delta\ell|}\sqrt{(A_2 - A_1\cos k\Delta\ell - B_1\sin k\Delta\ell)^2 + (B_2 + A_1\sin k\Delta\ell - B_1\cos k\Delta\ell)^2}, \\ a_R &= \frac{1}{2|\sin k\Delta\ell|}\sqrt{(A_2 - A_1\cos k\Delta\ell + B_1\sin k\Delta\ell)^2 + (B_2 - A_1\sin k\Delta\ell - B_1\cos k\Delta\ell)^2}. \end{aligned}\right\} \tag{5}$$

In the calculation, the dispersion relation of the following is presumed to hold:

$$\sigma^2 = gk\tanh kh. \tag{6}$$

Figure 24. Goda and Suzuki (1976) method of irregular wave analysis.

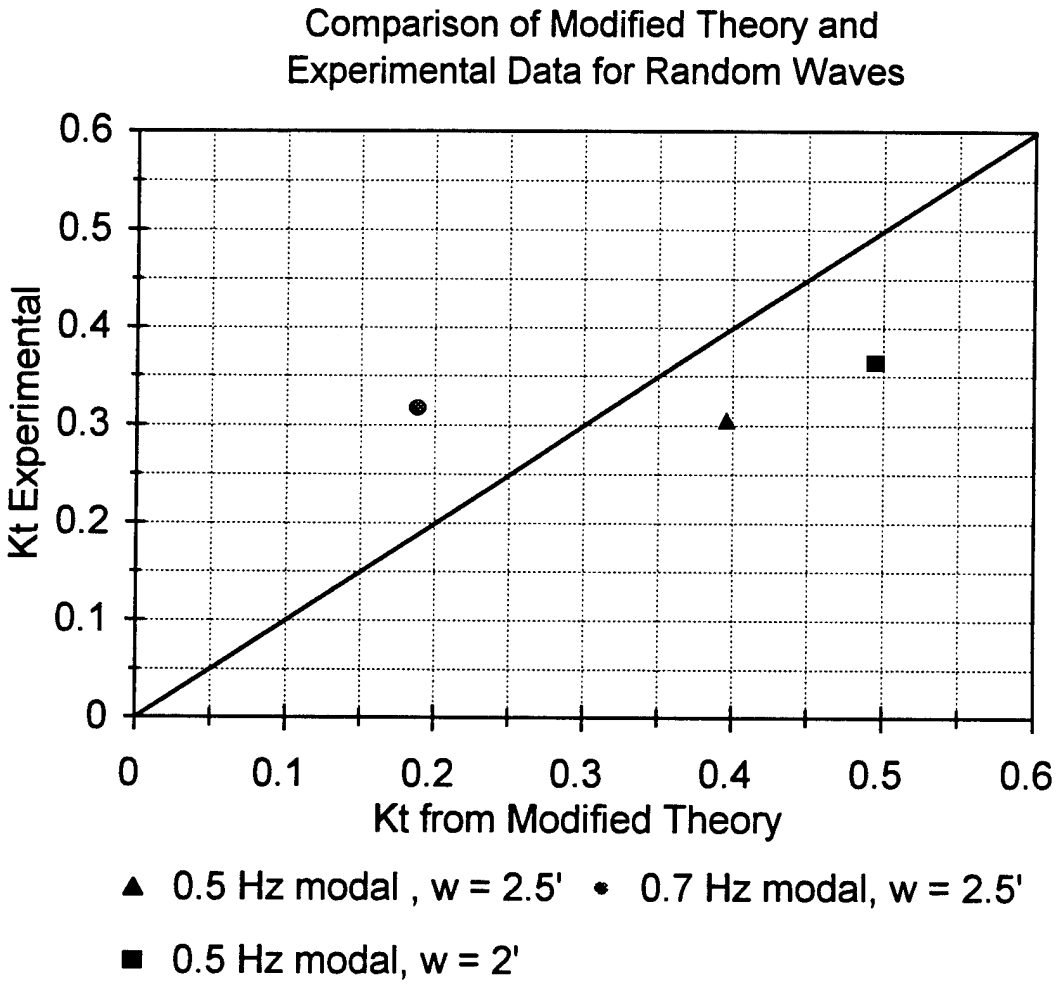

Figure 25. Comparison of K_t Experimental with K_t Theoretical for irregular wave tests on wave barrier.

components of the spectrum in the higher frequencies will have much smaller amounts of transmission. Thus, the overall coefficient of transmission for the wave spectrum will be smaller than modified theory suggests for regular waves for a 0.5 Hertz wave. While this difference is pronounced, it is not large due to the fact that only a small amount of the spectral energy will be distributed to those waves of frequency farthest from the peak. This reasoning explains the 0.5 Hertz test data, but at this time the 0.7 Hertz data trends cannot be accounted for.

WAVE FORCES -- REGULAR WAVES

Wave forces due to regular waves were recorded at the same time as data for transmission of regular waves and thus the setup and testing procedures follow those as outlined previously for the wave transmission. Forces were recorded individually near the top and bottom of the wave barrier using two force gages (Figure 18) and these measurements were then summed to determine a single, total force on the center test section. These total forces were then compared to predictions from the modified theory for forces (Equation 41) and the results are shown in Figure 26. Forces in the downtank direction (resulting from a wave crest at the wall) are positive and are denoted by a triangle. Forces obtained when a trough is at the wall are negative and denoted by an oval. The absolute values of the experimental forces were used in this graph. From Figure 26, it is apparent that the modified theory for computing forces is generally

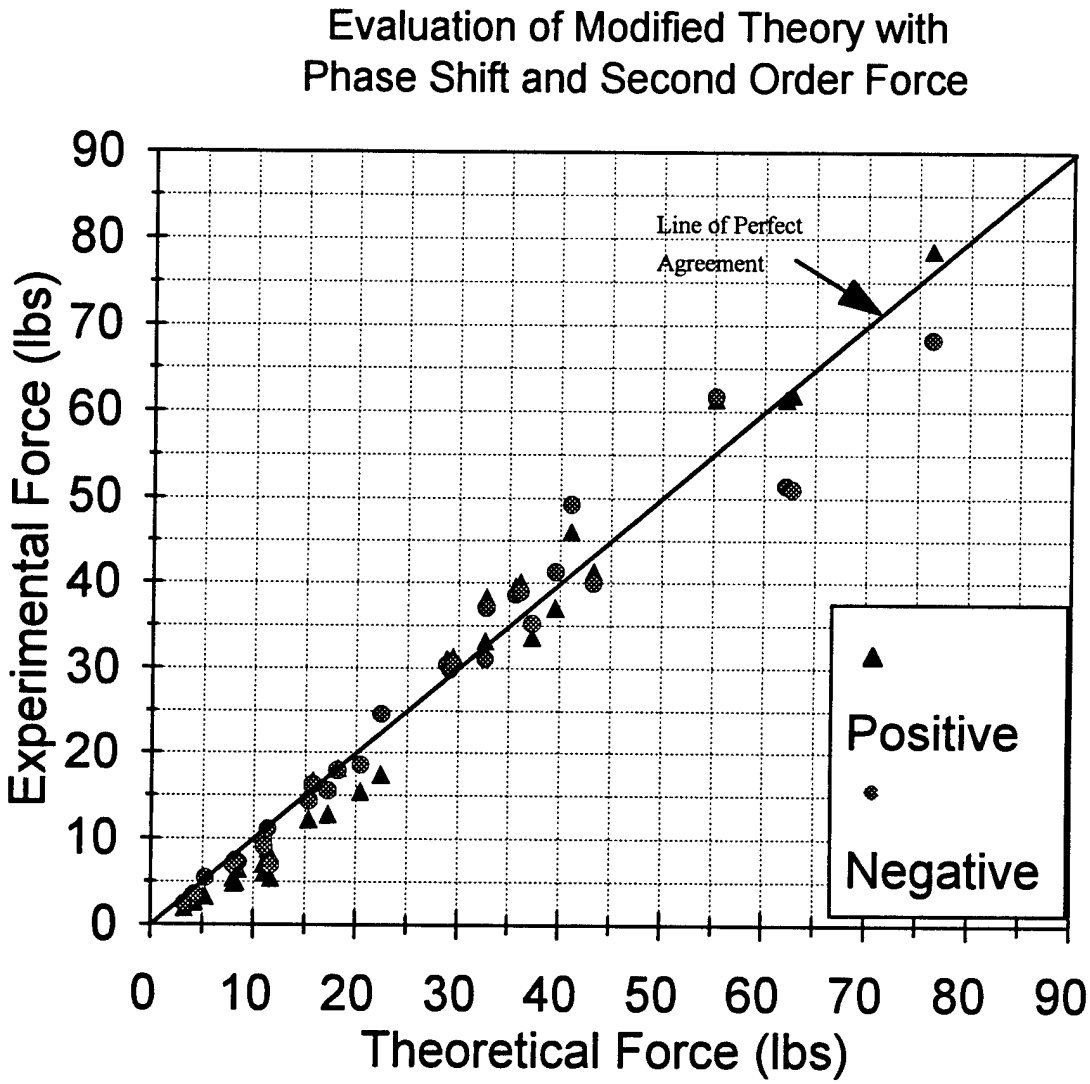

Figure 26. Comparison of experimental data to modified force theory predictions. waves.

accurate. Overall, the new theory provides relatively small errors in force prediction. This is especially true for the largest forces measured (from 30 to 80 lb due to 0.7 and 0.5 Hertz waves) where errors were less than 20%.

On average, the theory is slightly conservative. By applying linear regression theory to the experimental data, it was determined that experimental force was 98.7% of the experimental force. Most of the largest error occurred for 0.9 and 1.1 Hertz waves where measured forces were fairly small.

The testing matrix for regular wave tests developed two distinct situations when predicting forces. The first situation applies to 0.5 and 0.7 Hertz waves. These waves are long enough to transmit some of their energy under the barrier and the coefficient of transmission for these waves has an influence on how much force they exert on the barrier. These waves generally produced forces in excess of 25 pounds on the barrier and the modified theory had to account for the effects of the transmission and reflection of these waves. On the other hand, the transmission of the 0.9 and 1.1 Hertz waves was almost always equal to zero. The predicted coefficients of transmission and reflection therefore played no role in predicting the forces on the barrier at these frequencies. The predictions of the modified equation were still accurate, however. This shows the wide range of applicability of the modified theory because its accuracy does not vary with different ratios of wave barrier penetration relative to incident wave length or any other factors.

Figure 27 shows the results of using the NAVFAC method (NAVFAC, 1982) to compute the force on the model under test conditions. The NAVFAC force

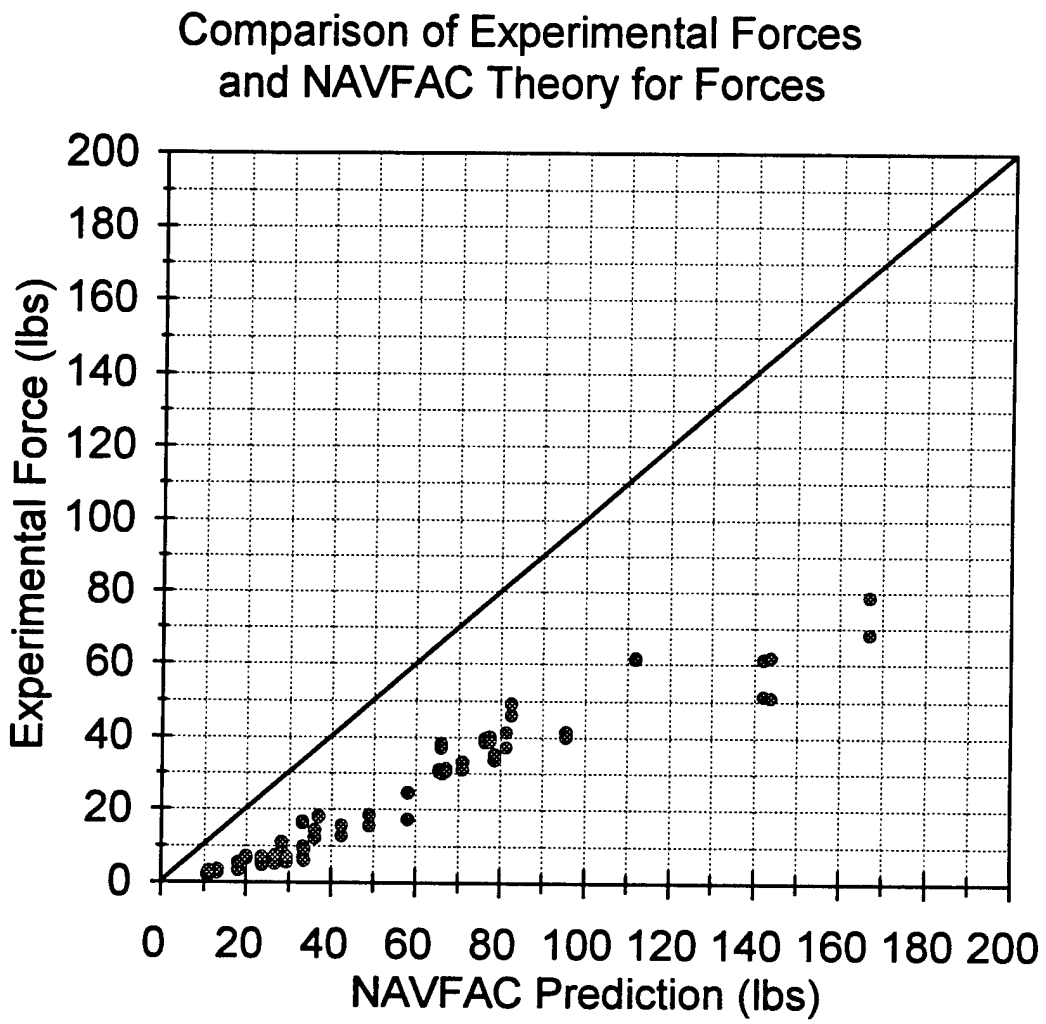

Figure 26. Comparison of NAVFAC predicted forces to experimental data for regular waves.

predictions differ considerably from those of the modified theory. In this case, forces are overstated by a factor of two to six (errors of 200% to 600%). This large error is a result of incorrect assumptions used in force computation by the NAVFAC manual. The largest source of error is due to the assumption that when a crest is acting on one side of a wall, a trough will be acting on the other side. For waves with significant amounts of transmission such as the 0.5 and 0.7 Hertz waves used in this project, this assumption will result in the overestimation of force by a factor of two to three. This error is due to the large pressure difference that results with an elevated water surface at the front of the wall and a depressed water surface behind the wall (assuming a crest at the front). As noted, observations of water levels recorded in this study show that there is always a 90 degree phase shift in water levels from the front to the back of the wall. When a crest is at the front, the zero crossing of the wave is at the rear, i.e. the water surface at the rear is at the still water level.

While this incorrect assumption can be the source of a large amount of error, another incorrect assumption can generate even larger factors of error. The NAVFAC method approximates dynamic pressure due to incident waves as a straight line when in actuality it is a hyperbolic relationship according to the linear wave theory for dynamic pressure (Equation 15). The NAVFAC method then further compounds this error for deep water waves (such as the 0.9 and 1.1 Hertz waves used in this experiment) by assuming that the dynamic pressure is equal to zero at the sea floor. In reality, dynamic pressure is equal to zero at the wave base. For waves with the wave base at a significant height above the sea floor, this assumption can result in large errors when the pressure is

integrated over the entire depth.

UNDERWALL FLOW TESTING

Fluid velocities in front of and under the wall were measured and recorded using an Acoustic Doppler Velocimeter at the positions shown in Figure 20. This series of testing utilized regular waves having a frequency of 0.5 Hertz, a wave steepness of 1/40, and a wall penetration of 2.5 feet. Particle velocities under the wall were examined to gain a better idea of the velocity and direction of flow underneath the wall.

Over a series of five waves, horizontal and vertical particle velocities were recorded. The magnitude of the velocity was then calculated for each pair of velocities and over a series of five waves the recorded velocities and magnitudes were averaged. Additionally, a least-squares-fit analysis was performed to determine the average error of each data run. A least-squares-fit error analysis examines an experimental data series such as that of particle velocity versus time. Through numerical analysis, amplitude coefficients are then calculated which, when multiplied by sine and cosine components, will approximate an "ideal" curve through a data series. The error at any point can be calculated by comparing the value of this "ideal" curve at a point with the value of the experimental data at the same point. This process was repeated at each grid point by generating another set of waves after moving the ADV probe to a location shown on the grid.

Particle velocities were plotted as a function of time and as a function of depth in order to compare flow at different points. As shown in Figure 28, water particle velocity under the wall did depend strongly on depth. There is a significant departure between particle velocity as predicted by theory and actual particle velocity in the area immediately below the wall. This departure exists because particles at this area cease to travel in their usual elliptical orbits. There is a net surge of water back and forth under the wave barrier due to the large pressure difference between the front and back of the wall. Water will flow from an area of higher pressure to lower pressure. Thus, when a wave crest is at the front of the wall dynamic pressures are at their maximum, water begins to flow from the front of the wall to the back of the wall. When there is a trough at the front of the wall the lower-pressure region is now in front and water will flow back to the front side of the wall. Figure 29 shows the turbulence in this back-and-forth flow beneath the bottom of the wall. Figure 30 is a graph of particle velocities at a greater depth than Figure 29 and shows the general smoothness of flow at greater depths. Flow at shallower penetrations is much more turbulent. This can be shown in two ways. First, the regular horizontal and vertical particle flow is more irregular at shallower depths. Second, there is a significant amount of motion in the Z- , or cross-tank, direction at shallower depths. Particle motions should be in only two-dimensions according to linear wave theory. The presence of a vortex as a result of turbulent flow could induce particle velocities in the Z-direction, however. It is this large amount of cross-tank flow that also helped to determine the size of the induced vortex in the next part of the project.

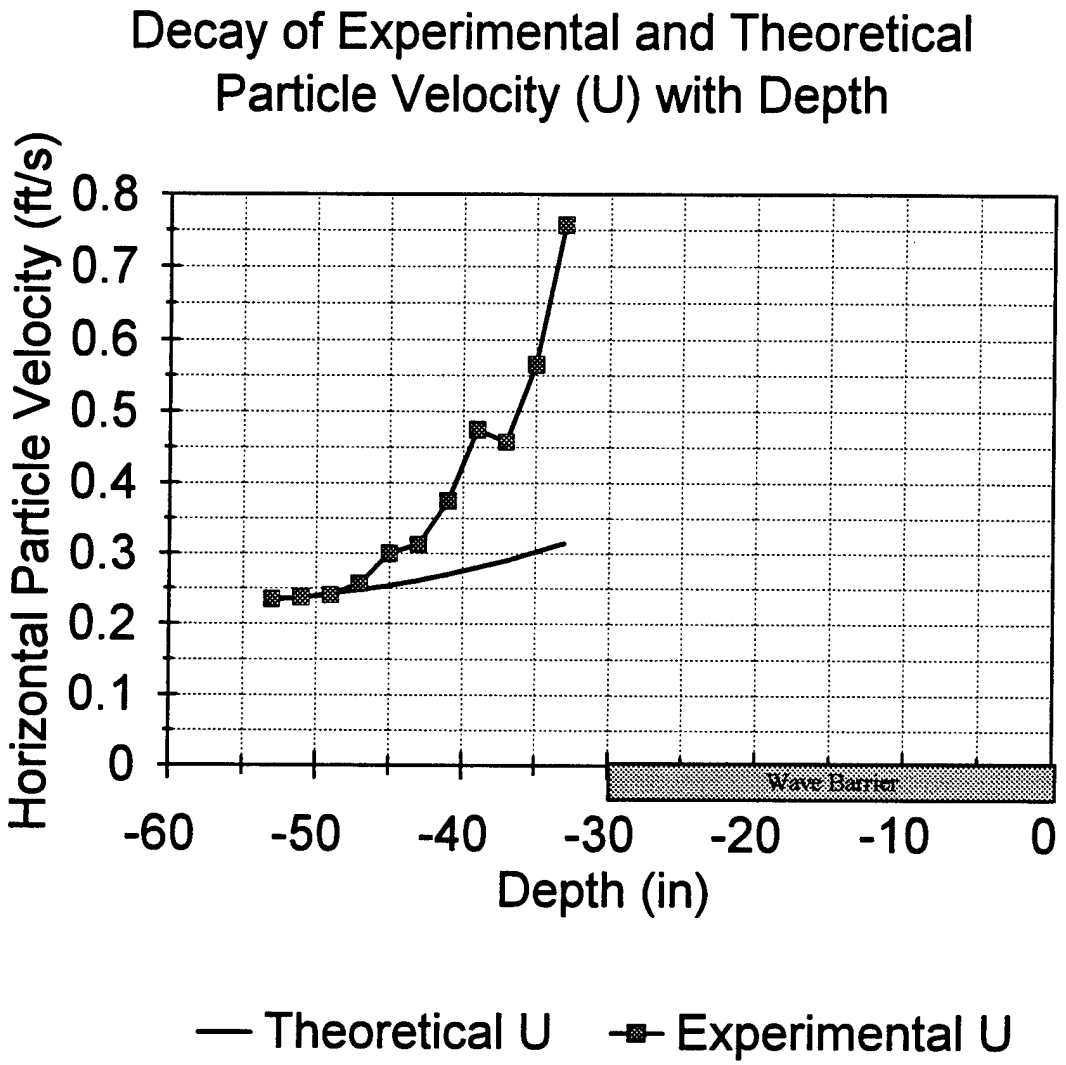

Figure 28. Graph of experimental and theoretical horizontal velocity (with wave barrier annotated) versus depth.

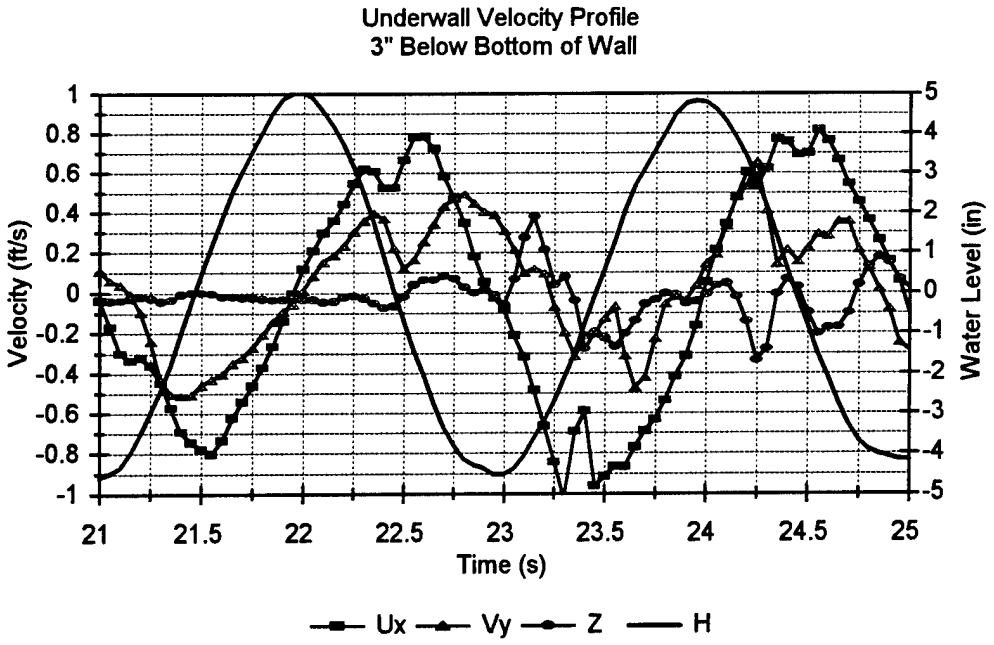

Figure 29. Graph of underwall particle velocity versus time at a penetration of 33 inches.

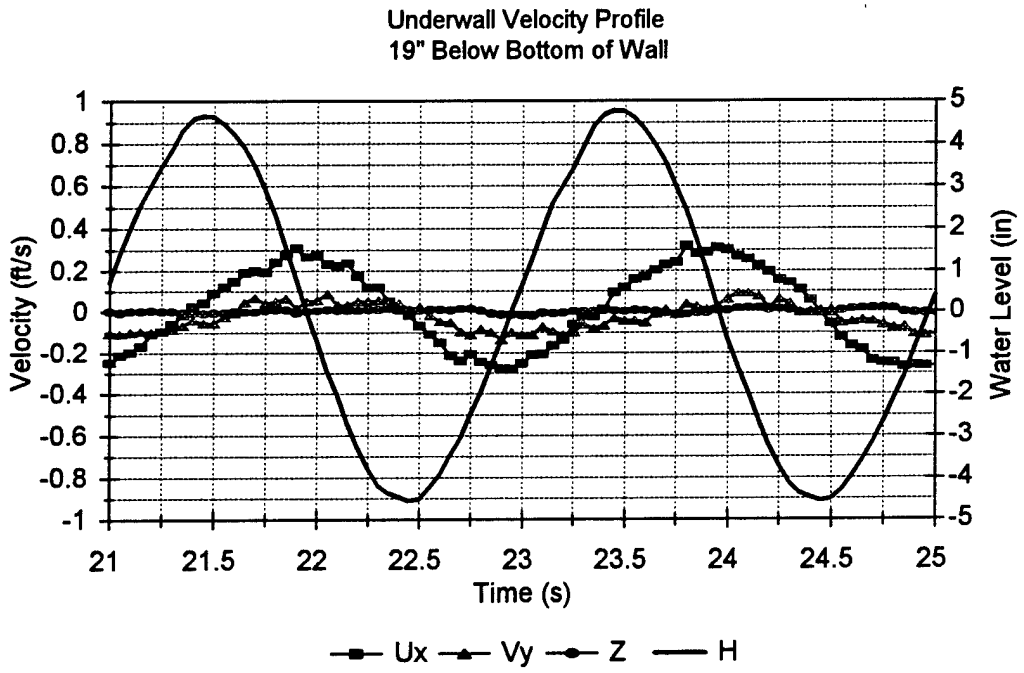

Figure 30. Graph of underwall particle velocity versus time at a penetration of 49 inches.

VORTEX FLOW TESTING

Vortex flow tests were performed under the same conditions as the underwall flow tests. The goal of this part of testing was to map the extent and magnitude of the vortex that forms from the irregular flow under the wall. Data from this phase were analyzed with the same methods as used in underwall flow analysis. A graph of least-squares-fit error at each testing point is shown in Figure 31.

This error was calculated by first computing the least-square fit of a 0.5 Hertz sine/cosine waveform to the velocity signals recorded during testing. The error between each measured data point and the best-fit sine/cosine curve was then calculated for all points and averaged. This mean error is the number next to each measurement point in Figure 31.

The calculation of the mean error can be used to map the vortex if it assumed that the deviation from the best-fit sine/cosine function is the result of turbulent flow. The presence of a baseline error seems to validate this assumption. If the points 45" and greater below the wall are examined, there appears to be an average error of approximately 0.01. By assuming this error to be the "background" or "baseline" error, a reference is gained for gauging the turbulence of the vortex in different areas.

The error in Figure 31 is largest in the area surrounding the bottom of the wall. The average error then decreases as points farther from this "pocket" are considered. This corresponds with fluid dynamics theory because vortices are supposed to lose energy as they move away from their point of origin. Thus the area where the vortices

are the strongest and would therefore generate the most error is immediately surrounding their point of origin, which in this case is the bottom of the wall. As points farther from this origin are examined, the error decreases, as would the energy of any turbulent flow as it approaches those points.

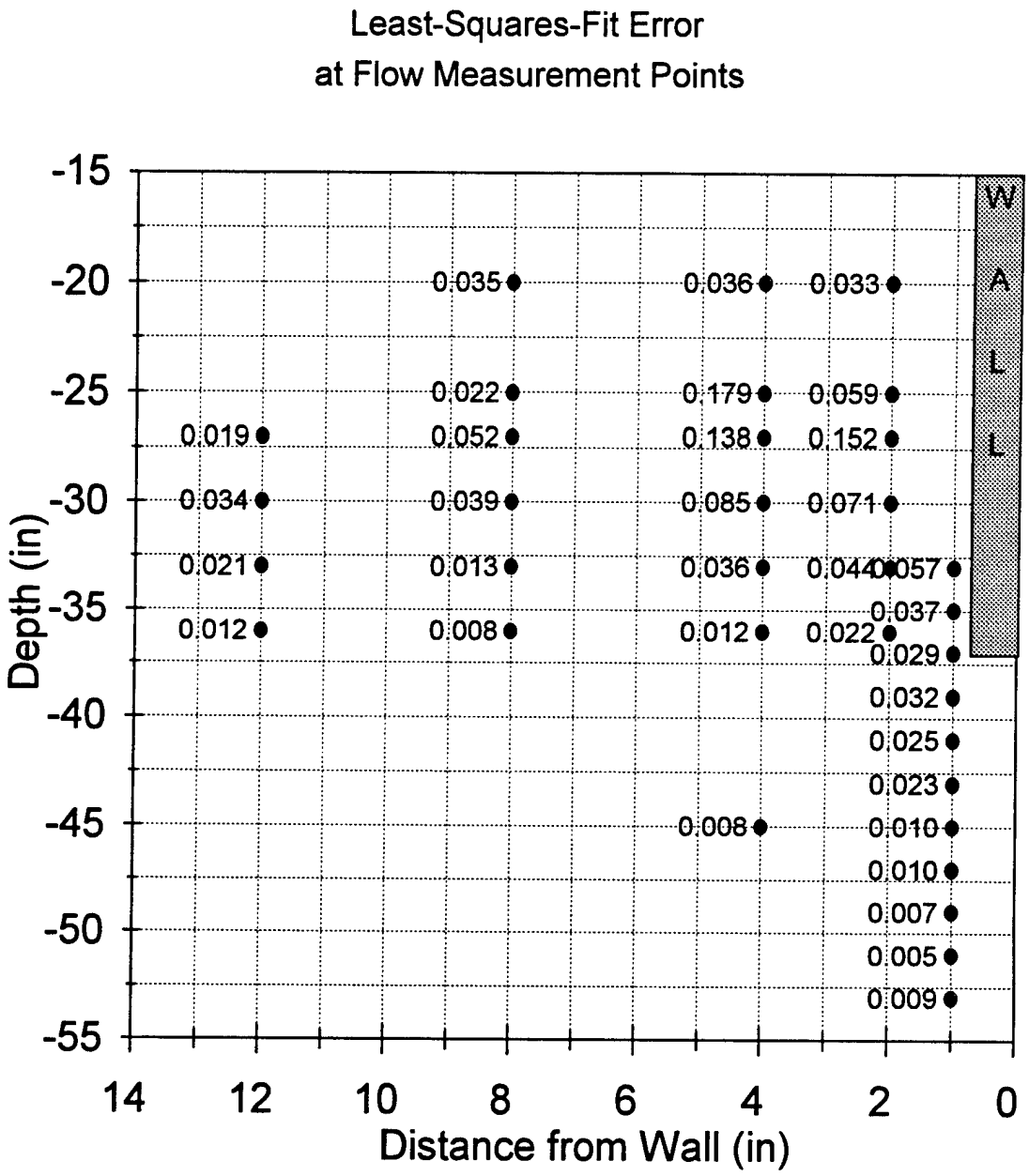

Figure 31. Graph of least-squares-fit error at test locations around wave barrier.

CONCLUSIONS

From the results of this study on vertical wave barriers, the following conclusions may be drawn:

- It is necessary to account for wave reflection when attempting to calculate wave transmission and forces. Wiegel theory does not account for reflection and its effects on particle velocity and wave pressures. This causes Wiegel theory to overestimate wave transmission.
- The modified theory for transmission is a valid improvement on existing methods of calculating wave transmission. The experimental data corresponded well with predicted values of transmission.
- There is a 90-degree phase shift in the water level between the front and back of a vertical wave barrier. This phase shift ensures that when there is either a crest or a trough at the front of a wave barrier, the water behind the wall will be at the still water level.
- First and second order dynamic forces and the 90-degree phase shift must be accounted for in the devlopment of a theory to predict forces on a wave barrier. The modified theory for wave forces includes these considerations and is a valid theory that can be expected to predict wave forces on a vertical wave barrier accurately.
- The existing NAVFAC method for computing forces on wave barriers is extremely conservative. The assumption of an 180-degree phase shift is incorrect, as is the assumption that dynamic pressures will extend to the seafloor instead of the wave base.

- The back-and-forth flow of water beneath a wave barrier is turbulent and induces the formation of vortices. These vortices act primarily in an area slightly above the bottom of a wave barrier.

- When analyzing vertical wave barriers, an assumption of conservation of mass should be used instead of conservation of energy. The formation of vortices from turbulent flow confirms that energy is not conserved during water flow beneath a wave barrer.

-The modified theories for transmission and wave forces significantly improve the prediction of wave transmission and the forces on a wave barrier. In addition, the modified theory for wave forces is much simpler and easier to use than the NAVFAC method for predicting force.

ACKNOWLEDGEMENTS

I would like to sincerely thank my Trident Advisor, Dr. David L. Kriebel, of the United States Naval Academy Naval Architecture, Ocean, and Marine Engineering Department. His wisdom and encouragement inspired me throughout the course of this project. Ms. Louise Wallendorf of the U.S. Naval Academy Hydromechanics Laboratory also gave much of her time and energy to my project in the design and testing phases. The rest of the Hydromechanics Laboratory staff, especially Mr. John R. Hill, Branch Head of the Hydromechanics Laboratory, Don Bunker, Steve Enzinger, John Zselesky, Norman Taylor, and Ensign Mike Roche, USN, deserve my hearty thanks as well. At times, moving and troubleshooting the wall required more muscle and brains than I could provide alone; they were always ready and willing to lend a hand. My roommate, Joel Ellingson, deserves a "hoo-yah" for living with me for three years; this year was definitely the worst. Most importantly, I would like to thank my parents Bret and Marlene Bollmann for giving me the tools and support I've needed to get where I am today. Any successes I have are really the result of what they have given me through the years.

REFERENCES

Gilman, J.F., 1995, Personal Communication.

Gilman, J. F. and Nottingham, D. (1992). "Wave Barriers: An Environmentally Benign Alternative," *Proceedings of Coastal Engineering Practice* '92, American Society of Civil Engineers, pp. 479-486.

Gilman, J. F. and Shaver, M. (1993). "Physical Model Study of a Pile-Supported, Thin, Rigid Wave Barrier," *Proceedings of Canadian Conference on Coastal Engineering*, Vancouver, B.C.

Goda, Y. and Suzuki, Y., 1976, "Estimation of Incident and Reflected Waves in Random Wave Experiments," *Proceedings of 15th Conf. On Coastal Engineering*, American Society of Civil Engineers, Vol. 1, pp. 828-845.

Losada, I. J., Loasada, M. A., and Roldan, A. J., 1992, "Propagation of Oblique Incident Waves Past Rigid Vertical Thin Barriers," Applied Ocean Research, Vol. 14, pp. 191-199.

Lott, J. W. And Hurtienne, W. E., 1992, "Design, Construction, and Performance of a Baffled Breakwater," *Proceedings of Coastal Engineering Practice*, American Society of Civil Engineers, pp. 486-502.

Matsson, B. And Cederwall, K., 1976, "Vertical Barriers as Wave Attenuators," International Association For Hydraulic Research, Stockholm.

Miche, R., "Mouvements ondulatoires de la mer in profendeur constante ou decroissante," *Annals des Ponts et Chaussees*, Paris, Vol. 114, 1944.

Naval Facilities Engineering Command, 1982, "Coastal Protection Design Manual 26.2," U.S. Government Printing Office, Washington, D.C.

Peratrovich, Nottingham, & Drage, Inc., Issue #30, undated, "Permeable Wave Barrier," Engineering Report, No. 30.

Peratrovich, Nottingham, & Drage, Inc., Issue #39, undated, "Alaska Science & Technology Foundation Wave Barrier Research," Engineering Report, No. 39.

Rundgren, L., "Water Wave Forces," Bulletin No. 54, Royal Institute of Technology, Division of Hydraulics, Stockholm, Sweden, 1958.

Sainflou, M., "Treatise on Vertical Breakwaters," *Annals des Ponts et Chaussees*, Paris, 1928. (Translated by W. J. Yardoff, U.S. Army Corps of Engineers.

Sorenssen, Robert M., 1993, "Basic Wave Mechanics for Coastal and Ocean Engineers," John Wiley and Sons, New York, NY.

U.S. Army Corps of Engineers, 1984, "Shore Protection Manual," 4th edition, U.S. Government Printing Office, Washington, D.C.

Wiegel, R. L., 1960, "Transmission of Waves Past a Rigid Vertical Thin Barrier," J. Waterways and Harbors Div., ASCE, 86 (WW1), pp. 1-12.